Geothermics 116 (2024) 102842

Contents lists available at ScienceDirect

Geothermics

journal homepage: www.elsevier.com/locate/geothermics

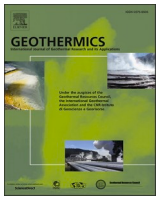

Contrasting influence of salt structures and faults on the geothermal potential of regional structural highs: The Cleaver Bank High, Southern North Sea

Qiang Zhang *, Tiago Alves

3D Seismic Lab, School of Earth and Environmental Sciences, Cardiff University, Main Building, Park Place, Cardiff CF10 3AT, United Kingdom

ARTICLE INFO

Keywords:
Salt structures
Faults
Geothermal potential
Cleaver Bank High

ABSTRACT

High-quality 3D seismic reflection data, complemented by 448 bottom-hole temperatures (BHTs) from 48 boreholes, are used to investigate the influence of salt structures and faults on the geothermal potential of the Cleaver Bank High, Southern North Sea. Developed salt structures include multiple salt diapirs, salt pillows and a salt wall, with their presence influencing local geothermal potential. Strata deposited above the Zechstein Group record geothermal gradients that are enhanced proportionally to the thickness of this salt unit. Conversely, strata buried below the Zechstein Group reveal a moderate decreasing trend in geothermal gradients as salt thickens. Large supra-salt faults can act as fluid paths to deep and hot fluid into shallow strata, resulting in the presence of high geothermal gradients in shallow strata. Importantly, geothermal gradients on the footwall of these faults are much higher than that on the corresponding hanging-wall, decreasing as one moves away from them. For example, average geothermal gradients on the footwall of the largest supra-salt fault (Fault A) are, relative to its immediate hanging-wall, 105 % higher in the North Sea Group, 26 % higher in the Chalk Group, and 41 % higher in the Rijnland, Upper and Lower Germanic Trias Groups. Additionally, sub-salt faults influence the geothermal gradient of supra-salt strata in parts of the study area where there is very thin, or even absent, salt (<100 ms; or ~230 m), forming distinct low-amplitude trails of fluid above these same faults. They also indirectly influence geothermal gradient by controlling the position, geometry and distribution pattern of salt structures. As a corollary, three potential geothermal exploration targets are suggested on the Cleaver Bank High, one located on the footwall of a large supra-salt fault, one above thick salt, and a third target above very thin Zechstein strata where low-amplitude fluid chimneys are found. The results in this work can be applied to similar salt-bearing structural highs in Northern Europe and worldwide.

1. Introduction

The use of geothermal energy for industrial and domestic purposes has increased for the past 35–40 years, accompanying an ever-rising demand for low-carbon energy (e.g. Gallup, 2009). Geothermal energy is considered as an important and potential resource in many a sedimentary basin (Erdlac et al., 2007; Busby, 2014; Daniilidis and Herber, 2017; Alves et al., 2022). Alas, its deployment is still limited when compared to other sources of energy due to its inherent high production and maintenance costs (Younger et al., 2012; Mijnlieff, 2020). In addition, geothermal energy sites are also often affected by some of the drilling hazards occurring in conventional oil and gas fields, at the same time requiring reliable, long lasting hydraulic yields and appropriate water temperatures (ideally beyond 150°C) to produce energy (Glaas et al., 2018; Vidal and Genter, 2018; Reinecker et al., 2019). Local geothermal gradient, reservoir architecture, lithology and industrial-scale water flow rate (or hydraulic yield) are particularly known geological factors controlling thermal energy output in many geothermal projects (Yang et al., 2000; Van Wees et al., 2012; Daniilidis and Herber, 2017; Reinecker et al., 2021).

A positive aspect concerns the fact that local geothermal gradients in sedimentary basins are greatly enhanced by the presence of buried salt intervals. This means that higher-than-normal temperatures occur above thick salt, and lower temperatures below, a phenomenon known as the 'chimney effect' (Jensen, 1983, 1990; Wilson and Ruppel, 2007; Canova et al., 2018; Nolan, 2021). Such an effect results from salt having a

* Corresponding author.
E-mail address: zhangq63@cardiff.ac.uk (Q. Zhang).

https://doi.org/10.1016/j.geothermics.2023.102842
Received 27 July 2023; Received in revised form 19 September 2023; Accepted 3 October 2023
Available online 14 October 2023

thermal conductivity that is two to four times greater than in other sedimentary rocks (Zhuo et al., 2016; Jackson and Hudec, 2017; Raymond et al., 2022). In parallel, faults in sedimentary basins, including salt-rich basins, can play an important role in focusing heat and fluid in the upper crust. They may act as favourable migration paths for deep and hot fluid, resulting in local temperature anomalies at shallow depths (Wood et al., 2001; Cloetingh et al., 2010; Hinz et al., 2014; McLean et al., 2018).

Salt structures are well developed on the Cleaver Bank High and include salt diapirs, pillows and walls. Salt diapirs and walls reflect the presence of ductile salt masses piercing their overburden, with salt walls being more elongated than salt diapirs (e.g. Jackson and Hudec, 2017). Salt pillows are upwellings of salt with a concordant overburden that is parallel to the upper salt contact (e.g. Jackson and Hudec, 2017). Salt structures on the Cleaver Bank High experienced multiple phases of growth, and their distribution was controlled by NW-striking sub-salt faults (Oudmayer and De Jager, 1993; Remmelts, 1995). These NW-striking sub-salt faults were intersected by conjugate NE-striking sub-salt faults, all of which record multiple phases of tectonic reactivation (Schroot and Haan, 2003; Ligtenberg et al., 2011; Van Ojik et al., 2020). In parallel, a large number of supra-salt faults are observed on the Cleaver Bank High, having accommodated local stresses resulting from prolonged halokinesis (Ten Veen et al., 2012; Zhang and Alves, 2023).

The aim of this paper is to investigate the influence of salt structures and faults on the geothermal potential of the Cleaver Bank High, as an

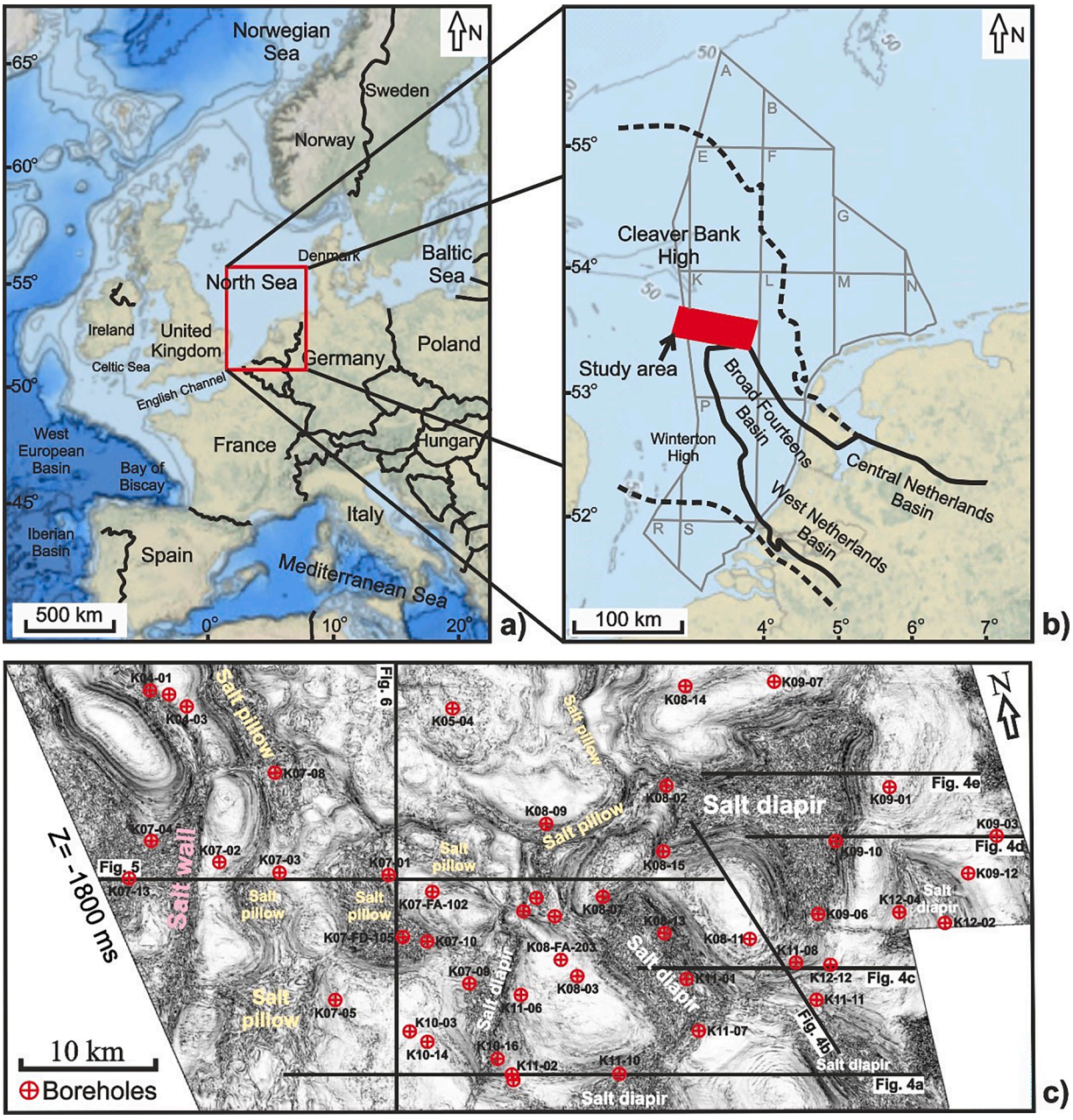

Fig. 1. (a) Bathymetric map of NW Europe and its continental margin. The red polygon highlights the location of Fig. 1b). (b) Bathymetric map showing the position of the Dutch sector of the Southern North Sea, as bounded by the grey polygon. The Broad Fourteens Basin, Central Netherlands Basin and West Netherlands Basin are highlighted by a black solid line, whereas the Cleaver Bank High and Winterton High are highlighted by a black dash line. The red rectangle marks the location of the 3D seismic volume. Bathymetric map is taken from the Bathymetric Data Viewer in National center for Environmental Information (https://www.ncei.noaa.gov/maps/bathymetry/). (c) Variance map ($Z = -1800$ ms two-way time) highlighting the position of different salt structures developed in the study area. The seismic profiles in Figs. 4–6 are shown as black lines.

example of a regional structural high in the Southern North Sea. In summary, this work addresses the following research questions:

(a) Is there an influence of salt structures on the geothermal potential of regional structural highs, such as the Cleaver Bank High?
(b) How do faults developed on structural highs control the geothermal potential of sub- and supra-salt strata?
(c) What potential geothermal exploration targets can be identified on the Cleaver Bank High?

2. Geological setting

The Cleaver Bank High is an important hydrocarbon producing area of the Southern North Sea in which gas is produced from both Westphalian and Upper Rotliegend sandstones (Fattah et al., 2012) (Fig. 1a). It spans ~8000 km^2 and bounds the Broad Fourteens Basin to the north (Quirk, 1993) (Fig. 1b and c). The Cleaver Bank High was first part of a foreland basin during the Variscan orogeny and was later affected by multiple tectonic episodes (Ziegler, 1990; De Jager, 2007) (Fig. 2). Importantly, the Zechstein Group decouples the Permian Rotliegend Group below from Triassic-Holocene strata above (Stewart and Coward, 1995; Ten Veen et al., 2012; Alves and Elliott, 2014). Previous work identified multiple basement fault trends beneath the Zechstein Group, the main evaporitic unit in the Southern North Sea (Schroot and Haan, 2003; Ligtenberg et al., 2011).

2.1. Upper palaeozoic

During the Carboniferous, the Cleaver Bank High was located in a foreland position relative to the Variscan orogen, and became the locus of important sedimentation (Limburg Group; Ziegler, 1990; De Jager, 2007). The Variscan orogeny, the tectonic event responsible for the closure of the Proto-Tethys Ocean, imposed a general N-S compressional regime along northern Europe at the end of the paleozoic (Devonian and Early Carboniferous; Schroot and Haan, 2003; Van Ojik et al., 2020). At this time, three different fault trends (E-W, NW-SE and NE-SW), inherited from older basement weakness zones, became active on the Cleaver Bank High (Schroot and Haan, 2003).

At the end of the Carboniferous, tectonic subsidence on the edges of the Variscan orogen preceded regional thermal uplift and igneous underplating, phenomena that resulted in the erosion of Upper Carboniferous strata (Fattah et al., 2012). In some areas, more than 1000 m of the Carboniferous Coal Measures were eroded below a regional Base Permian Unconformity (Quirk, 1993). Older fault were also reactivated in the latest Carboniferous-Early Permian, forming large-scale NE-SW and NW-SE conjugate fault systems (Ziegler, 1990).

Thermal cooling and regional subsidence predominated in the study area after latest Carboniferous-Early Permian tectonics. Aeolian, fluvial sediments and desert-lake deposits were deposited in the Late Permian as part of the Rotliegend Group (Van Wees et al., 2000; Doornenbal and Stevenson, 2010) and subsequently covered by evaporites, carbonates and clays in the Zechstein Group, which reflect a late period of crustal

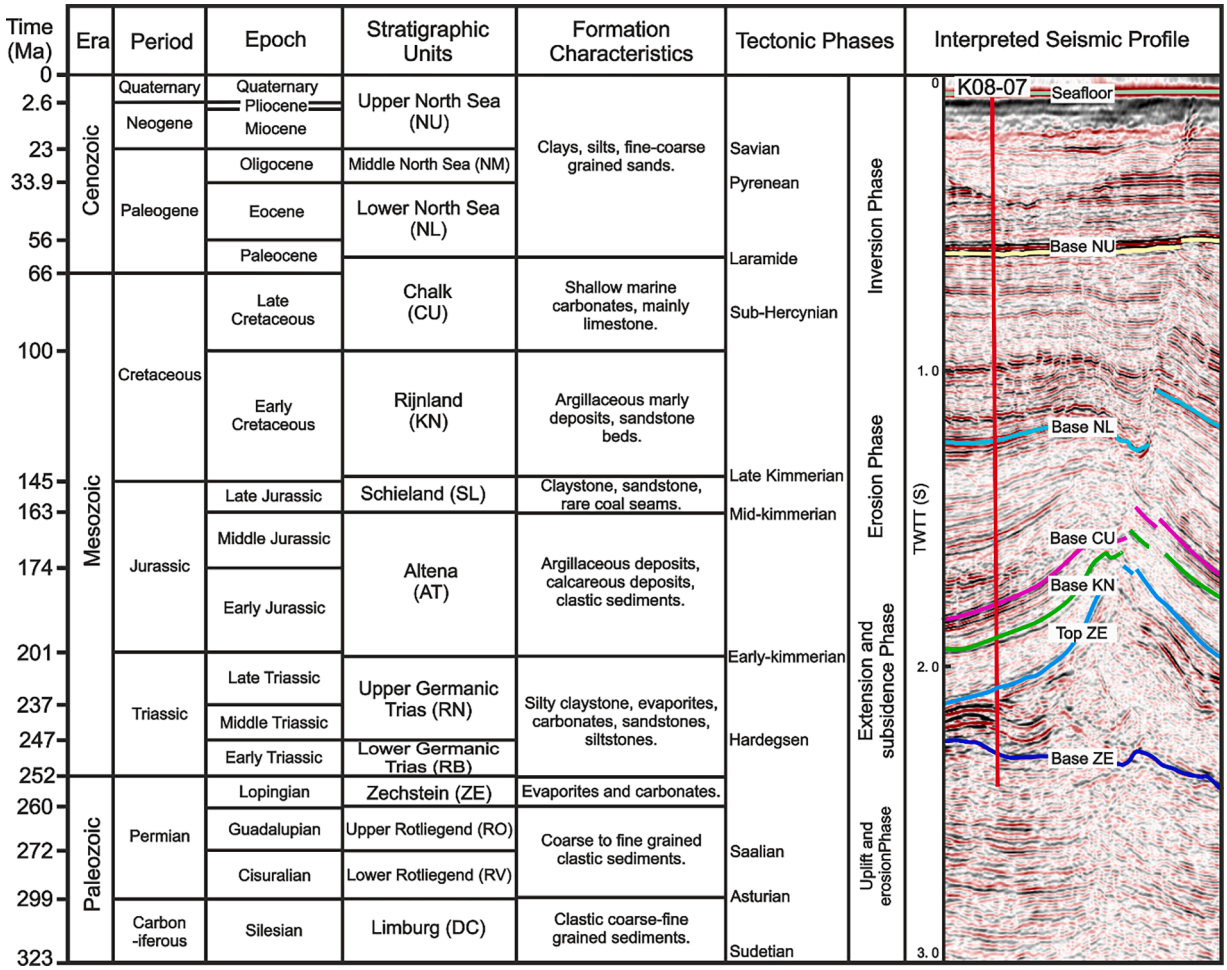

Fig. 2. Tectono-stratigraphic chart for the Cleaver Bank High summarising main stratigraphic units and their character (from Harding and Huuse, 2015). Multiple tectonic events and four tectonic evolutionary phases are highlighted. Seven important seismic-stratigraphic horizons, correlated with data from well K08–07, are shown on the seismic profile.

extension and subsidence (Fattah et al., 2012). On the Cleaver Bank High, tectonic extension followed a E–W direction during the Permian (Van Ojik et al., 2020).

2.2. Mesozoic

The Triassic was marked by E-W extension (Ziegler, 1990) and, consequently, the Cleaver Bank High records the accumulation of silty claystone, minor evaporites, carbonates and sandstones in the Upper and Lower Germanic Trias Group (Fig. 2). Extension near the study area still followed an E-W direction during the Early Jurassic (Early Kimmerian tectonic phase), and thus controlled the deposition of the Altena Group within the Broad Fourteens Basin (Fig. 2). Halokinesis started at this time, promoting structural decoupling between sub- and supra-salt strata (James, 2003).

Thermal doming and uplift of the Cleaver Bank High occurred in the Middle and Late Jurassic (Ziegler, 1990; De Jager, 2007). This tectonic phase was associated with continental rifting and resulting sea-level fall, causing widespread erosion of structural highs in the Southern North Sea; the so-called Mid and Late Kimmerian phases (Ziegler, 1990; De Jager, 2007; Ten Veen et al., 2012). On the Cleaver Bank High, Upper Triassic and Lower Jurassic strata are completely absent (Quirk, 1993).

Sea level rose once again during the Early Cretaceous and the study area was gradually flooded. As a result, siliciclastic intervals in the Rijnland Group (Fig. 2) accumulated over Triassic strata and, locally, the Zechstein Group (Schroot and Haan, 2003). The main direction of extension was reoriented to NE-SW from the Late Kimmeridgian to the Early Cretaceous (Deckers and van der Voet, 2018).

Regional thermal subsidence prevailed in the Late Cretaceous and a thick succession of limestones, the Chalk Group, was subsequently deposited (Fattah et al., 2012) (Fig. 2). The Alpine orogeny was initiated in Central Europe at this same time due to convergence of the African and Arabian plates with Eurasia (De Jager, 2007; Fattah et al., 2012). This resulted in the onset of NW-SE tectonic compression on the Cleaver Bank High. Moderate halokinesis occurred due to this same compression, as suggested by the local thinning of the Chalk Group strata towards salt structures.

2.3. Cenozoic

On the Cleaver Bank High, Cenozoic sediments are unconformable over the Chalk Group. They consist of clays, silts and fine to coarse sands (Fig. 2). Two inversion episodes affected the study area during the Paleogene; the Mid-Paleogene Pyrenean and the Late Paleogene Savian tectonics. Apatite fission-track data show that the Cleaver Bank High was locally uplifted during the Pyrenean inversion (Alberts et al., 1991). In contrast, Savian tectonic inversion was milder and marked by a broad, regional unconformity separating Paleogene from Neogene strata (Chen, 2016). During the Cenozoic, the main direction of compression remained orientated NW-SE, and reverse faults, thrusts and pop-up structures were locally formed (Van Ojik et al., 2020). In addition, salt movement occurred in the Eocene-Oligocene, accompanying tectonic inversion (Glennie, 1997; Harding and Huuse, 2015; Deckers et al., 2022). Major fold structures cored by salt pillows were initiated or amplified during the multiple Cenozoic tectonic phases (Stewart and Coward, 1995; Stewart, 2007; Ten Veen et al., 2012; Hernandez et al., 2018).

3. Data and methods

3.1. Seismic, borehole and temperature data

This work uses a three-dimensional (3D) seismic reflection volume from the Cleaver Bank High (Southern North Sea), complemented by 448 bottom-hole temperatures (BHTs; see Supplementary File 1) gathered from forty-eight (48) exploration boreholes (Fig. 1). The seismic volume was acquired in the southern end of the Cleaver Bank High, a structural high bordering the Broad Fourteens Basin to the north, and covers an area of ~2120 km^2 with an average water depth of 35 m (Fig. 1). Inline and crossline spacings for the seismic data are 25 m, as they have been processed with a 25 × 25 m bin size. Stratigraphic and P-wave velocity (V_p) data, obtained from boreholes tied to discrete seismic reflections, reveal a minimum vertical resolution ($\lambda/4$) ~40 m below the main salt unit in the study area, and ~12 m in the shallowest Cenozoic strata. The seismic data are zero-phased and displayed using the European SEG polarity convention, in which an increase in acoustic impedance is shown as a red seismic reflection, while a decrease in acoustic impedance coincides with black seismic reflections (Brown, 2001).

Apart from BHTs, the 48 wells drilled in the study area provide Gamma Ray (GR), Lithology, Density (RHOB) and Sonic (DT) data. Hence, well correlations are completed in this work to identify lithological variations and establish a chronostratigraphic framework for the interpreted seismic-stratigraphic units (Figs. 2 and 3). Hence, five (5) key seismic-stratigraphic units are defined and correlated with borehole data (Figs. 3 and 4). Thickness maps for four (4) of these units are compiled to highlight major thickness variations associated with halokinesis and tectonic inversion. In addition, fault maps from four (4) key horizons, superimposed on the areas where the Zechstein Group is >400 ms, highlight any relationships amongst faults and salt structures.

BHTs are systematically corrected in this work due to the fact that raw BHTs obtained from the well geophysical logs are usually cooler than true formation temperatures (e.g. Chapman et al., 1984; Deming, 1989). Importantly, a total of 12 BHTs (out of 448) acquired from sonic cement bond logs (CBLs) effectively represent the true formation temperature - CBLs commonly run from days to years after drilling, recording the maximum BHT read by a thermometer, or probe (Holgate, 2005). These 12 BHTs have not been corrected as highlighted in Supplementary File 1.

The remaining 436 BHTs (out of 448) are corrected by applying the modelling tools provided by ZetaWare, Inc (Corrigan, 2003). These tools include three correction methods for BHTs; the Horner correction, the Time-Since-Circulation correction and the Last-Resort correction (Corrigan, 2003). The Horner correction can be used when three of more self-consistent BHTs from a given depth are available, with this correction involving the plotting of BTHs in a given well vs. time (Chapman et al., 1984). Based on a study of 983 BHTs and associated equilibrium temperature estimates (T_{eq}), the T_{eq} uncertainty (1 sigma) using the Horner correction is ± 8 °C (Corrigan, 1997).

Time-Since-Circulation corrections are suggested when time-since-circulation information is available but deemed unsuitable for the Horner correction (Corrigan, 2003). With the Time-Since-Circulation correction, uncertainty in T_{eq} estimates (1 sigma) is in the order of ± 6–12 °C with a post-circulation time of 10 h, decreasing to ± 3–6 °C with a post-circulation time of 30 h (Corrigan, 2003).

When only BHTs are available with no time-since-circulation information, a Last-Resort correction is recommended by simply adding 18°C to the original temperatures (Corrigan, 2003). For the Last-Resort correction, the expected T_{eq} uncertainty is ± 9 °C (Corrigan, 2003).

Based on the T_{eq} uncertainty caused due to three correction methods, the Horner correction for BHTs performs better than the Time-Since-Circulation correction. The Time-Since-Circulation correction for BHTs has a lower uncertainty in T_{eq} than the Last-Resort correction. Thus, the Horner correction for BHTs is chosen over the Time-Since-Circulation correction, and the latter is chosen over the Last-Resort correction.

In this work, only three (3) out of 436 BHTs data are suitable for the Horner correction method. A total of 242 BHTs are suitable to be corrected by using the Time-Since-Circulation method, and the remaining 191 BHTs are simply corrected based on the Last-Resort correction method. The detailed correction method used for each BHT has been listed in Supplementary File 1. In addition, measured depths (MDs) of 96 BHT data recorded from inclined boreholes are converted into true vertical depths (TVDs). Finally, corrected BHTs are tied in this work to

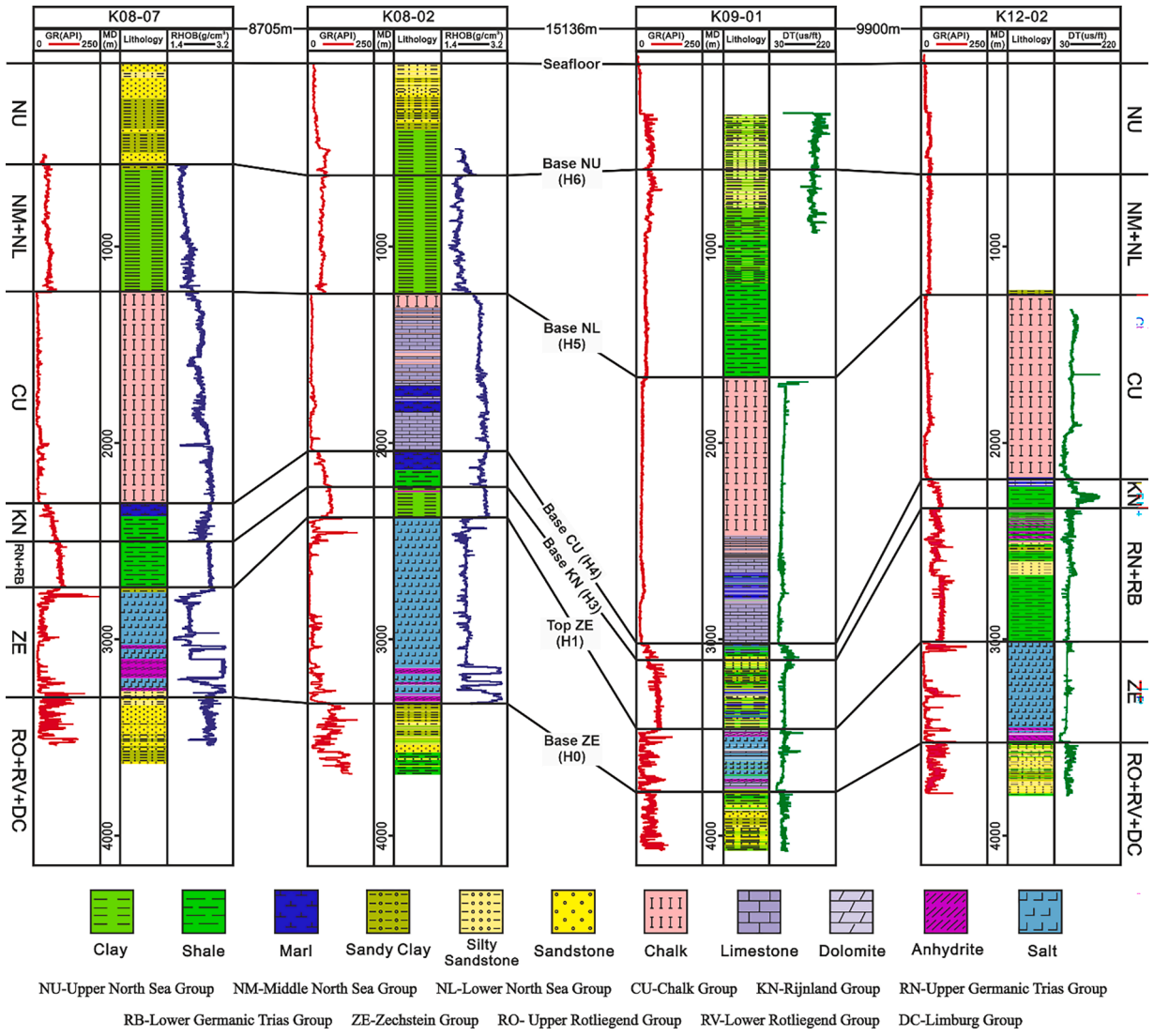

Fig. 3. Stratigraphic correlation for wells K08–07, K08–02, K09–01 and K12–02 located in the study area. Stratigraphic framework, lithology, gamma-ray (GR), density (RHOB) and sonic log (DT) wireline curves are shown.

the five interpreted seismic-stratigraphic units, so as to ensure that each of these units has more than 20 corrected BHTs.

3.2. Correlations amongst BHTs and main lithostratigraphic units

Most wells terminate below the Zechstein Group, so this work was able to separate the Upper Rotliegend and Limburg Groups in terms of their geothermal potential. Geothermal gradients are calculated considering the seafloor temperature as 7.8°C at the present-day water depth of 35 m (Defant, 1961; Evans and Coleman, 1974).

Normal probability plots are compiled to calculate P90, P50 and P10 probabilities for the corrected BHTs and geothermal gradients in each stratigraphic unit (Table 1). P90 means that there is, at least, a 90 % probability that the values will equal or exceed the low estimate for BHTs or geothermal gradients; P50 indicates at least a 50 % probability that the values estimated will equal or exceed the best estimate for BHTs and geothermal gradients; P10 represents a 10 % probability of the calculated values to equal or exceed the higher estimate for BHTs and geothermal gradients. In addition, vertical depth is plotted against corrected BHT and geothermal gradient to highlight any depth-dependent changes.

Subsidence and thermal models (1D modelling on PetroMod® 2021) for wells K11–10, K11–02 and K12–12 are used to investigate the burial and thermal histories of the Cleaver Bank High. Stratigraphic units recorded in well completion logs, and their corresponding lithologies, are obtained from the Dutch Oil and Gas portal (NLOG) (see Supplementary File 2). Main uplift and erosion phases are considered in the study area, especially the Saalian and Mid-Late Kimmerian events. The amount of eroded material is estimated based on the erosion maps published by Fattah et al. (2012), assuming that the depositional thicknesses of the Step Graben Formation, the Hospital Ground Formation, the Altena Group, the Upper Germanic Trias Group and the Lower Germanic Trias Group are 50, 200, 200, 400 and 500 m, respectively. Palaeo-water depth curves are also compiled based on the published literature (Fattah et al., 2012) as well as the lithologies and depositional environments recognised for specific units. The palaeo temperature at the sediment water interface (SWIT) is calculated with an integrated PetroMod tool, which considers palaeowater depth and the evolution of ocean surface temperatures through time depending on the palaeolatitude of the study area.

Basal heat flow is based on the work of Fattah et al. (2012), where values for well K01–02 were calculated using the 1D tectonic heat flow modelling tool PetroProb (Van Wees et al., 2009). Importantly, well K01–02 is close to wells K11–10, K11–02 and K12–12 in this work, at a distance of ~ 45 km, and reveals similar geological conditions and burial histories to those of the Cleaver Bank High. Thermal conductivity values

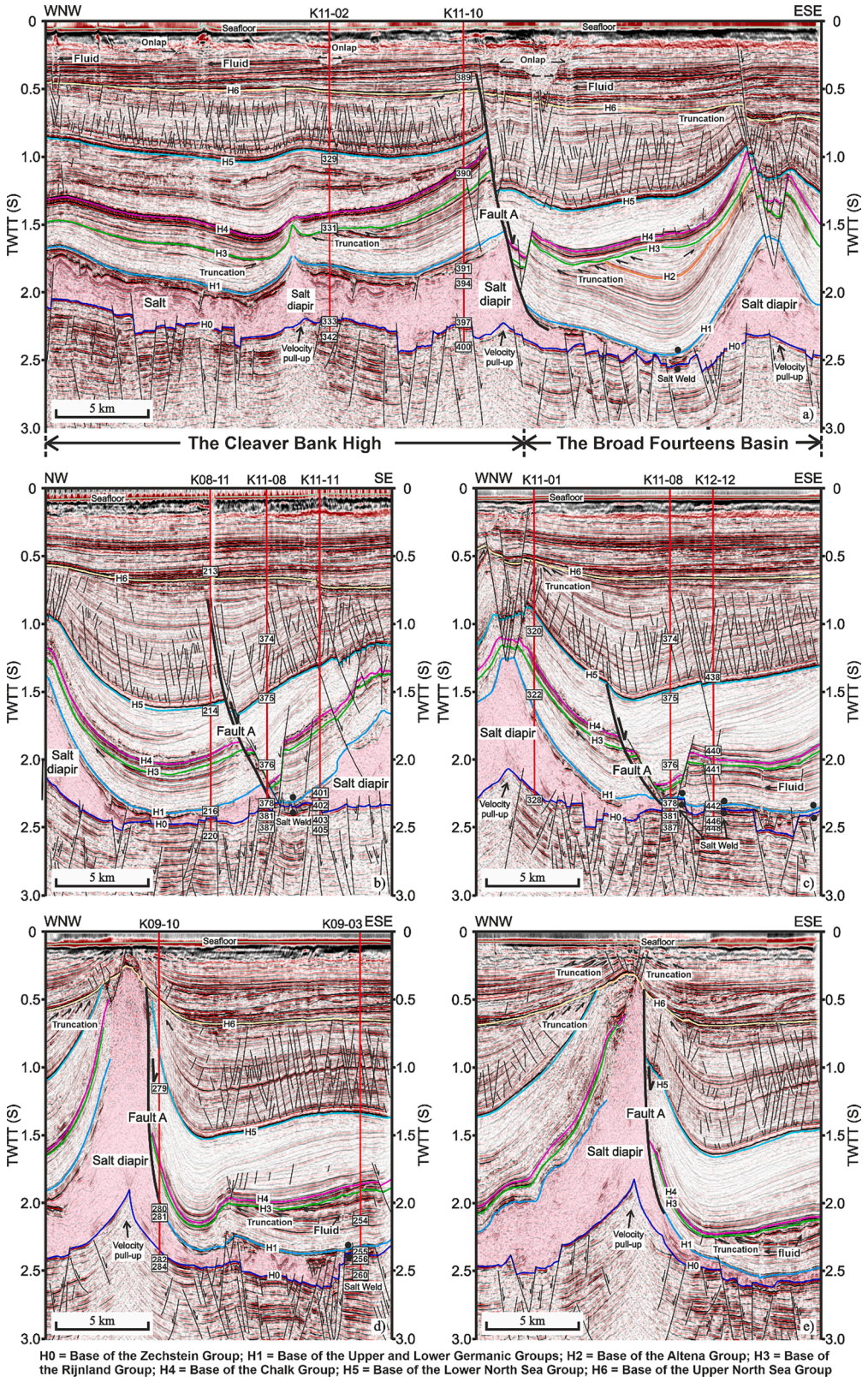

Fig. 4. TWTT seismic profiles across the largest NE-striking supra-salt fault (Fault A), showing multiple salt structures, faults and fluid flow paths. Eight seismic horizons tied to data from eight exploration wells are shown by different colour lines and labels, while faults are shown as black lines. The figures highlight the two largest salt diapirs in the study area, which are bounded by a large supra-salt fault, Fault A. This fault separates the Cleaver Bank High from the Broad Fourteens Basin. Salt diapirs have irregular geometries, different heights and widths. The location of the seismic profiles is shown in Fig. 1c. Labels on the borehole trajectories indicate the depth of BHTs numbered in Supplementary File 1.

Table 1
Corrected BHTs and geothermal gradients for different stratigraphic units calculated using normal probability plots.

	Stratigraphy units	Well Number	Number of BHT data	P90		P50		P10	
				Corrected BHT (°C)	Gradient (°C/km)	Corrected BHT (°C)	Gradient (°C/km)	Corrected BHT (°C)	Gradient (°C/km)
Supra-salt strata	North Sea Group (Seismic Unit 5)	13	22	50.7	42.0	61.4	63.1	72.1	84.1
	Chalk Group (Seismic Unit 4)	23	42	57.8	33.3	76.2	47.0	94.7	60.6
	Rijnland, Upper and Lower Germanic Trias Groups (Seismic Unit 3)	14	24	76.0	32.9	94.5	40.6	113.1	48.4
Zechstein salt	Zechstein Group (Seismic Unit 2)	39	123	92.6	30.1	108.5	35.2	124.4	40.2
Sub-salt strata	Upper Rotliegend Group (Seismic Unit 1)	28	74	112.6	30.3	121.7	32.8	130.9	35.2
	Limburg Group (Seismic Unit 1)	44	163	114.6	30.6	125.3	32.9	136.0	35.2
	Supra-salt strata	35	88	54.4	31.7	77.5	49.3	100.7	66.8
	Sub-salt strata	48	237	113.8	30.5	124.2	32.9	134.6	35.2
	All stratigraphic groups	48	448	84.7	27.2	110.7	36.7	136.7	46.2

are calculated in this work based on a pre-defined thermal conductivity model - the Sekiguchi Model on PetroMod® 2021. Radiogenic heat production is calculated for the rock matrices for each of the lithologies. The compaction model is based on the Hydrostatic Athy's law Model where the porosity versus depth curve is a theoretical curve that assumes a hydrostatic pressure and a uniform lithological column. The initial geological model does not include faults and assumes open fluid flow boundaries. Temperature simulations run assuming hydrostatic conditions and only conductive heat flow is assumed in the model. Salt movement and, as a consequence, any related thermal effects are not considered in the models. Nevertheless, modelled present-day temperatures and corrected BHTs are provided, and these are able to highlight the temperature differences between them, and the influence of faults on local temperatures. Vertical thermal conductivities are shown, indicating the influence of lithology variations on geothermal gradients.

Temperature and geothermal gradient maps are compiled for specific stratigraphic intervals so to highlight the influence of salt structures on geothermal potential. Temperature maps are calculated using BHTs gathered around the horizon of interest, within an interval 200 m above or below this latter. Average geothermal gradients are used to compile geothermal gradient maps when there is more than one temperature measurement for a particular stratigraphic interval. We note that anisotropy effects of deviated wells were not considered when compiling these maps; hence, temperature and geothermal gradient maps compiled in this work are not 100% precise. Nevertheless, corrected BHTs and geothermal gradients from wells located around faults, mostly vertical wells, are recorded in two specific tables, highlighting the influence of specific structures on the geothermal potential of the study area (Tables 2 and 3).

4. Seismic stratigraphic units

4.1. Unit 1 (Pre-Zechstein units)

Unit 1 is bounded at its top by horizon H0, a high-amplitude seismic reflection that correlates with the base of the Zechstein Group (Figs. 2 and 4). Its base is delimited by the acoustic basement, which occurs at a depth of ~3000 ms two-way travel time (twtt). Unit 1 comprises a ~750 ms thick package with low- to high-amplitude seismic reflections. Sub-salt strata, especially those below thick salt, are usually of low amplitude and show local velocity pull-ups (Figs. 4–6).

Most wells drilled in the study area terminate within the Upper Rotliegend or Limburg Groups. Dominant lithologies include sandstone, sandy clay and shale. Gamma-ray and density values change dramatically with depth, indicating sharp lithological changes in these two stratigraphic groups (Fig. 3). Sub-salt faults are ubiquitous, and most propagate upwards through horizon H0. However, their lower tips are usually hard to observe in seismic data as many sub-salt faults propagate below the acoustic basement (Figs. 4–6).

4.2. Unit 2 (Zechstein group)

Unit 2 is the primary seismic interval of interest to this study, correlating directly with the Zechstein Group. Its base coincides with horizon H0, whereas its top is horizon H1, a high-amplitude reflection (Figs. 4–6). Unit 2 consists of chaotic to transparent seismic reflections, though it locally shows distinct high-amplitude reflections. The thickness of Unit 2 varies from 0 ms in salt welds to over 1600 ms in salt diapirs (Figs. 4–6 and 8).

Unit 2 is mainly composed of salt with low gamma-ray and density values (Fig. 3). However, its upper boundary includes a thin layer of claystone, which in some areas presents high gamma-ray values and low density values (Fig. 3). Dolomite stringers – the high-amplitude features previously mentioned as occurring within salt – are also observed in Unit 2, but are fragmented and gently folded. Faulting is common at its base, but its top is less compartmentalised, except in the northern part (Figs. 7 and 9). In some areas where thin salt exists, large sub-salt faults propagate into supra-salt strata (Fig. 4).

4.3. Unit 3 (Rijnland, upper and lower Germanic Trias Groups)

Unit 3 is bounded at its base by horizon H1, whereas its top is delimited by horizon H4, a high-amplitude reflection correlating with the base of the Chalk Group (Figs. 4–6). On the Cleaver Bank High, Unit 3 includes the Rijnland (KN), Upper (RN) and Lower (RB) Germanic Trias groups, plus the Altena Group (AT) in the small portion of the Broad Fourteens Basin covered by the 3D seismic volume (Fig. 4a). The Altena and Rijnland Groups are bounded at their bases by horizons H2, H3, respectively (Fig. 4–6). Unit 3 consists of low-amplitude to transparent seismic reflections in its lower part, changing to high-amplitude seismic reflections at its top. Seismic reflections are often truncated beneath the Rijnland Group, marking an angular unconformity between the Rijnland and the Germanic Trias Groups (Figs. 4-6). The thickness of Unit 3 ranges from 0 to 900 ms, showing a marked increase towards the south (Fig. 8).

Unit 3 consists of shales and marls, but thin anhydrite has also been drilled at particular locations (Fig. 3). Variable gamma-ray and density values dominate this unit. Faults are not common, except for a few large faults, and crestal faults above salt structures (Figs. 4–7). Nevertheless, small faults are developed around the base of Unit 3 in the northern part of the study area (Figs. 7 and 9).

4.4. Unit 4 (Chalk group)

The base of Unit 4 coincides with horizon H4, and its top with horizon H5, a high-amplitude reflection that correlates with the base of the

Table 2
Corrected BHTs and geothermal gradients recorded from twelve (12) wells located next to Fault A, highlighting the influence of this fault on local geothermal gradient. The highest geothermal gradient and its corresponding corrected BHT are listed below when there is more than one temperature measurement for a seismic-stratigraphic unit. Well locations are shown in Figs. 1c and 4.

Well Name	Position	Distance to the fault (m)	Thickness of the Zechstein salt (m)	North Sea Group		Chalk Group		Rijnland, Upper and Lower Germanic Trias Groups		Zechstein Group		Upper Rotliegend Group		Limburg Group	
				Corrected BHT (°C)	Gradient (°C/km)	Corrected BHT (°C)	Gradient (°C/km)	Corrected BHT (°C)	Gradient (°C/km)	Corrected BHT (°C)	Gradient (°C/km)	Corrected BHT (°C)	Gradient (°C/km)	Corrected BHT (°C)	Gradient (°C/km)
K11–10	Footwall	2450	1283	46.9	121.8	–	–	78.4	65.4	104.7	48.5	–	–	128.0	33.8
K11–02	Footwall	9526	899	–	–	67.1	67.9	82.3	44.1	–	–	116.4	34.6	118.8	33.0
K11–07	Hanging wall	566	722	–	–	88.1	48.0	–	–	81.0	36.6	101.0	34.1	119.8	34.3
K11–01	Footwall	2623	1493	–	–	77.5	60.9	89.1	49.3	–	–	–	–	–	–
K08–11	Footwall	2586	132	52.8	84.0	87.9	49.5	–	–	117.5	34.0	–	–	119.8	31.1
K11–11	Hanging-wall	3472	396	–	–	–	–	–	–	109.5	33.5	–	–	123.6	31.2
K11–08	Hanging-wall	806	77	65.0	54.3	67.4	39.0	–	–	113.8	32.0	121.4	33.0	124.0	31.8
K12–12	Hanging-wall	2373	83	71.2	45.9	101.0	36.0	–	–	95.0	31.8	125.0	32.4	122.0	30.8
K09–06	Footwall	–	1709	–	–	–	–	–	–	87.4	44.6	117.3	31.5	125.0	31.3
K12–04	Hanging-wall	5501	182	–	–	73.4	46.8	119.8	37.5	–	–	128.0	33.0	131.1	33.8
K09–10	Footwall	–	1781	–	–	54.8	44.7	–	–	98.9	42.9	115.4	29.0	–	–
K09–07	Footwall	6093	486	–	–	80.3	44.4	–	–	113.4	32.3	115.0	32.9	132.8	37.0
Average values for footwall		4656	1112	49.9	102.9	73.5	53.5	83.3	52.9	104.4	40.5	116.0	32.0	124.9	33.2
Average values for hanging-wall		2544	292	68.1	50.1	82.5	42.5	119.8	37.5	99.8	33.4	118.9	33.1	124.1	32.4
Difference (%) for footwall to hanging-wall		83	281	−27	105	−11	26	−31	41	5	21	−2	−3	1	3

Table 3
Corrected BHTs and geothermal gradients measured from wells located next to two large NW-striking cresta faults above a salt pillow, a fluid path and a large hard-linked fault (Fault B). The highest geothermal gradient and its corresponding corrected BHT are listed below when there is more than one temperature measurement for a seismic-stratigraphic unit. Well locations are shown in Figs. 1c, 5 and 6.

Well Name	Position	Distance to the fault (m)	Thickness of the Zechstein salt (m)	North Sea Group		Chalk Group		Rijnland, Upper and Lower Germanic Trias Groups		Zechstein Group		Upper Rotliegend Group		Limburg Group	
				Corrected BHT (°C)	Gradient (°C/km)	Corrected BHT (°C)	Gradient (°C/km)	Corrected BHT (°C)	Gradient (°C/km)	Corrected BHT (°C)	Gradient (°C/km)	Corrected BHT (°C)	Gradient (°C/km)	Corrected BHT (°C)	Gradient (°C/km)
K07–01	Structural high	–	954	65.3	100.5	–	–	87.0	41.6	–	–	–	–	123.8	34.2
K07-FD-105	Structural high	–	1192	26.7	72.8	47.0	50.5	77.3	39.1	107.0	42.8	–	–	117.0	31.8
K10–03	Salt withdrawal basin	–	650	67.1	68.8	98.0	58.6	–	–	98.0	38.5	–	–	121.1	34.9
K09–03	Next to fluid path	–	182	–	–	–	–	129.0	40.6	134.0	31.6	116.0	31.4	139.7	35.4
K07–13	West of Fault B	4274	1365	–	–	42.6	65.6	–	–	64.3	32.3	–	–	125.0	35.1
K07–02	East of Fault B	1751	228	–	–	–	–	83.0	33.7	–	–	108.7	33.1	120.9	34.3

Lower North Sea Group (Figs. 4–6). Unit 4 comprises low-amplitude to transparent seismic reflections in the eastern part of the study area, changing to moderate- to high-amplitude seismic reflections in the west. Its thickness is relative uniform, with an average value of 650 ms, though local strata thinning is observed near salt structures (Figs. 4–6).

Unit 4 is mainly composed of chalk and limestone with low gamma-ray and high density values (Fig. 3). Thin marl intervals have also been drilled in its interior. Similarly to Unit 3, faults are scarce, except above salt structures (Figs. 4–7).

4.5. Unit 5 (North sea group)

Unit 5 is bounded at its base by horizon H5, whereas its top coincides with the seafloor (Figs. 4–6). This unit includes the Upper (NU), Middle (NM) and Lower (NL) North Sea Groups. The base of the Upper North Sea Group is marked by horizon H6. Its thickness ranges from 100 to over 1600 ms, showing low-amplitude to transparent seismic reflections in its lower part, but moderate- to high-amplitude seismic reflections towards the top. Strata in Unit 5 thins out on the flanks of salt structures, especially next to the large salt diapirs (Figs. 4 and 8).

Unit 5 is composed of siliciclastic sediments, with high gamma-ray and low density values in its lower part, but low gamma-ray in its upper part (Fig. 3). The unit comprises claystone and shale in its lower part, but sandy clay and sandstone in its upper part. Faulting is common in its lower part, especially where polygonal faults are present, but most are delimited by horizon H6. There are also multiple cresta faults above salt structures, propagating from Unit 4 (Figs. 4 and 6).

5. Salt structures and fault families on the Cleaver Bank High

5.1. Geometry and distribution of salt structures

Salt structures on the Cleaver Bank High experienced multiple phases of growth, with their geometry and distribution revealing obvious differences. Salt diapirs are mainly developed in the eastern and south-eastern sectors of the study area, showing triangular or sub-circular shapes in plan view (Fig. 1). Salt diapirs mainly strike to the NW and NE, similarly to sub-salt faults (Figs. 7–9).

The two largest salt diapirs in the study area are bounded by a large NE-striking supra-salt fault separating the Cleaver Bank High from the Broad Fourteens Basin (Figs. 4, 7 and 9). This fault is herein named ‘Fault A’ as it is one of the main structures in the study area. In seismic data, salt diapirs have irregular geometries with differing heights and widths (Fig. 4). Their height ranges from ~700 to over 1600 ms twtt that is much higher than salt pillows (Fig. 8d).

Salt pillows are developed in the western and middle sectors of the study area, showing rhomboid to rectangular shapes in plan view (Fig. 1). Similarly to the salt diapirs mentioned above, they are also NW- to NE-striking. On seismic profiles, they overlie many NW- and NE-striking sub-salt faults (Figs. 4–6 and 9). Their heights vary from 200 to 850 ms twtt, values that are lower than those of the salt diapirs (Figs. 5 and 6). In addition, a single salt wall occurs in the western sector of the study area in association with a large NE-SW strike-slip fault (Figs. 1 and 5). This large strike-slip fault is herein named ‘Fault B’ as it is one of the main structures in the study area. The salt wall has a width of ~2.5 km, spanning a limited area in the study area. The salt wall shows a taper shape on seismic profiles, and is ~700 ms twtt tall (Figs. 4–6).

5.2. Faults developed on the Cleaver Bank High

Faults are common on the Cleaver Bank High, and can be separated into three groups based on their spatial distribution and stratigraphic position relative to the Zechstein Group: (a) sub-salt, (b) supra-salt and (c) hard-linked faults. Supra-salt faults are faults developed above the Zechstein Group. Sub-salt faults are faults developed beneath the Zechstein Group, and do not cross its top boundary. Hard-linked faults

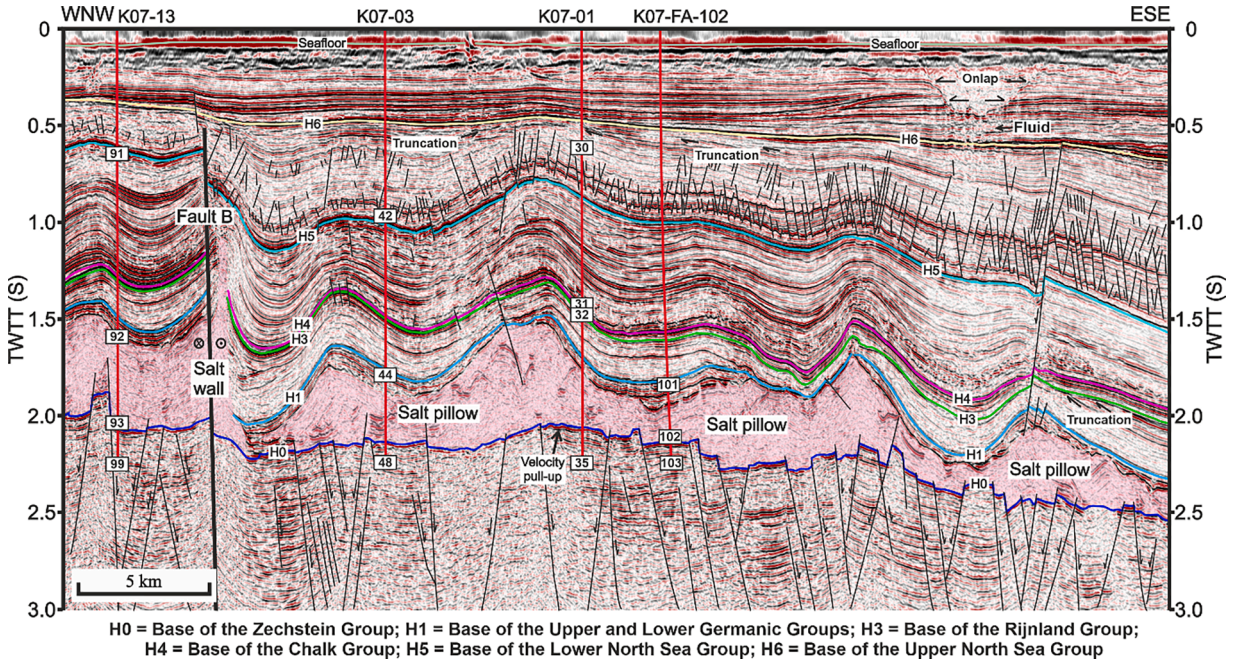

Fig. 5. TWTT seismic profile across the largest NE-striking hard-linked fault (Fault B), showing multiple salt structures, faults and fluid-flow features. Seven seismic horizons tied to data from four wells are shown by different colour lines and labels, while faults are shown as black lines. Fault B is a large NE-striking dextral strike-slip fault, which is near vertical and propagated from sub-salt units into the North Sea Group. Salt pillows and wall have shown different geometries, heights and widths. The location of the seismic profile is shown in Fig. 1c. Labels on the borehole trajectories indicate the depth of BHTs numbered in Supplementary File 1.

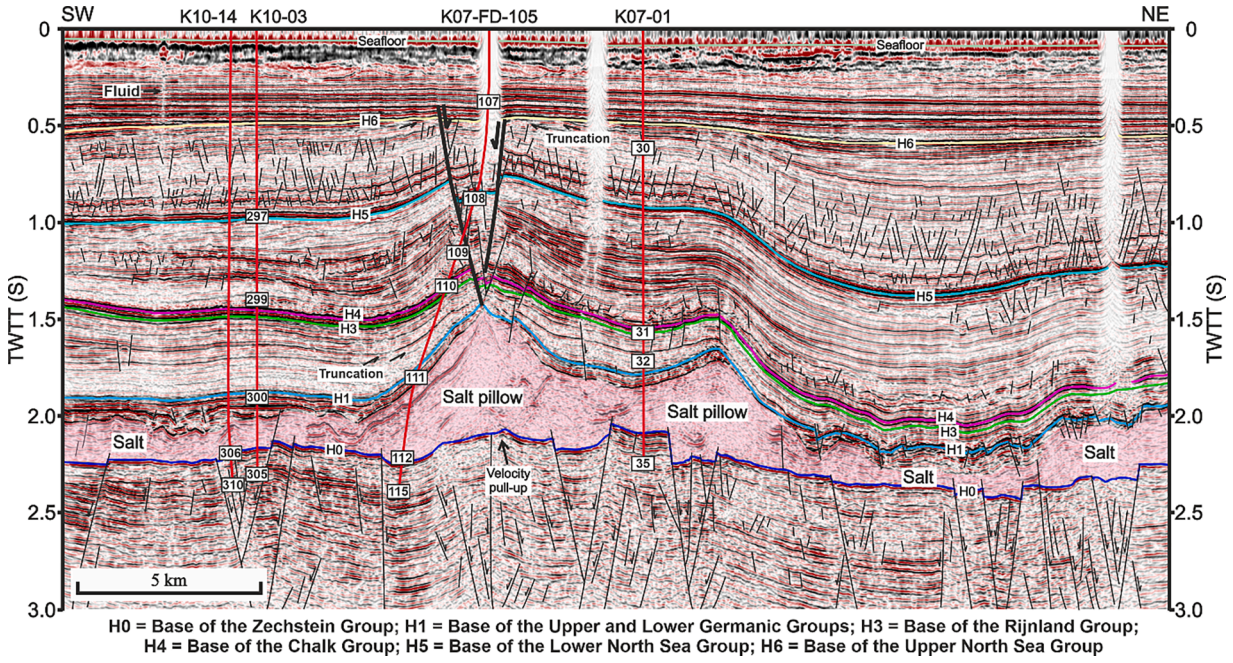

Fig. 6. TWTT seismic profile across the large NW-striking crestal faults, showing multiple salt structures and faults. Seven seismic horizons tied to data from four wells are shown by different colour lines and labels, while faults are shown as black lines. Two large crestal faults are imaged near Well K07-FD-105, propagating into the Upper North Sea Group. These crestal faults influence the geothermal gradient distribution around the salt pillows in the figure, as Table 3 denotes high geothermal gradients next to these faults. The location of the seismic profile is shown in Fig. 1c. Labels on the borehole trajectories indicate the depth of BHTs numbered in Supplementary File 1.

are faults originating beneath the Zechstein Group that propagate directly, or are linked, to structures in supra-salt strata.

5.2.1. *Supra-salt faults*

A large number of supra-salt faults are developed in the study area, but most are restricted to the North Sea Group, especially the Middle and Lower North Sea Groups (Figs. 4–7). Faults in the North Sea Group were formed in the Cenozoic, and include salt-related and polygonal faults (Figs. 4–7 and 9). Salt-related faults are developed around salt structures, accommodating the stress produced due to the growth of these structures (Zhang and Alves, 2023). Their length usually ranges from 400 to 3500 m, and their maximum displacement between 14 and 90 m.

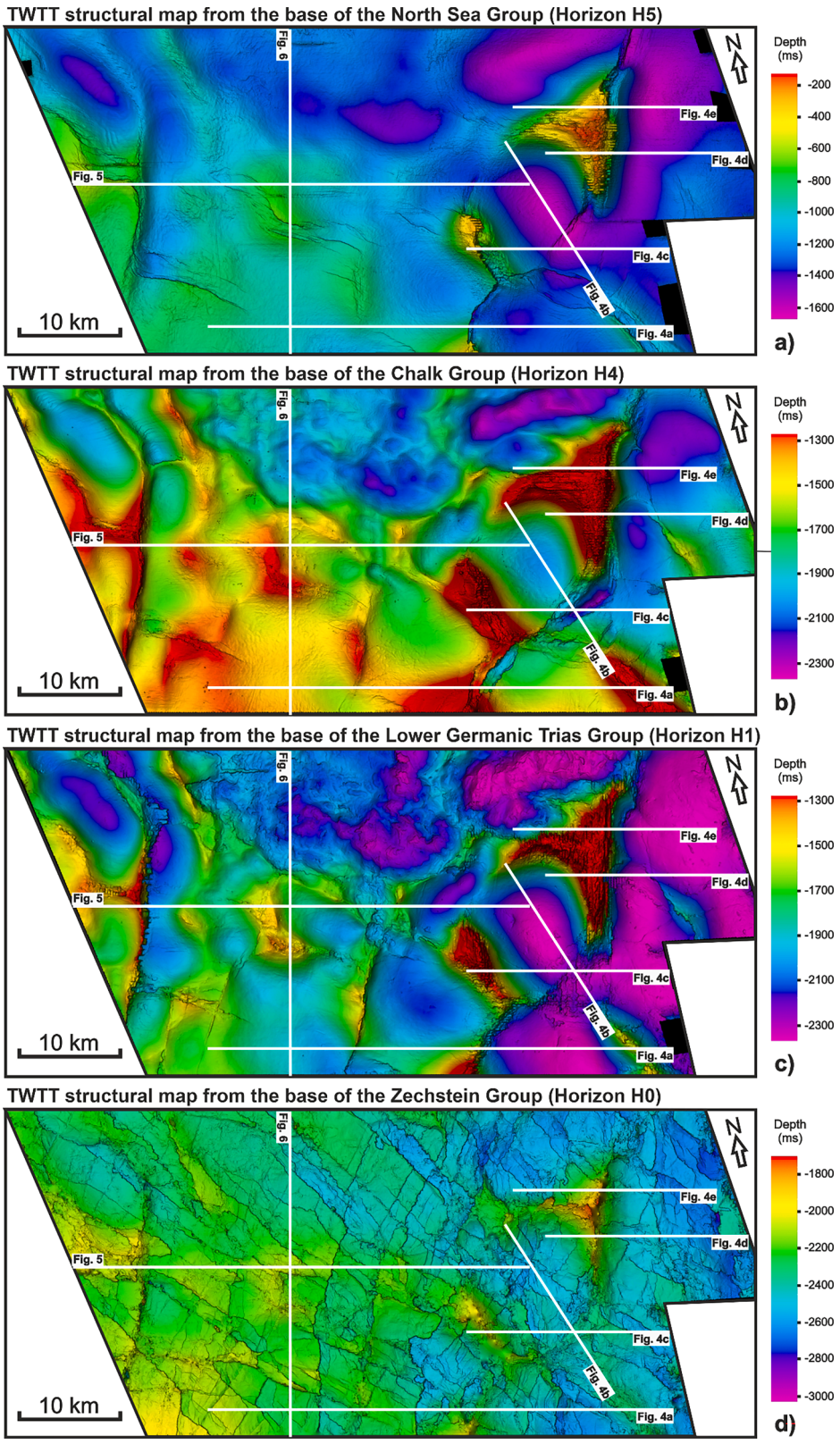

Fig. 7. TWTT structural maps for four key horizons in the study area, including the base of the North Sea Group (Horizon H5), Chalk Group (Horizon H4), Lower Germanic Trias Group (Horizon H1) and Zechstein Group (Horizon H0), respectively. (a-c) Maps with the position and spatial distribution of salt structures and supra-salt faults, highlighting the influence of halokinesis on the depth variation of overlying horizons. (d) Map showing the spatial distribution of sub-salt faults that mainly consist of NW- and NE-striking faults. The location of the seismic profiles shown in Figs. 4–6 is shown by the white lines.

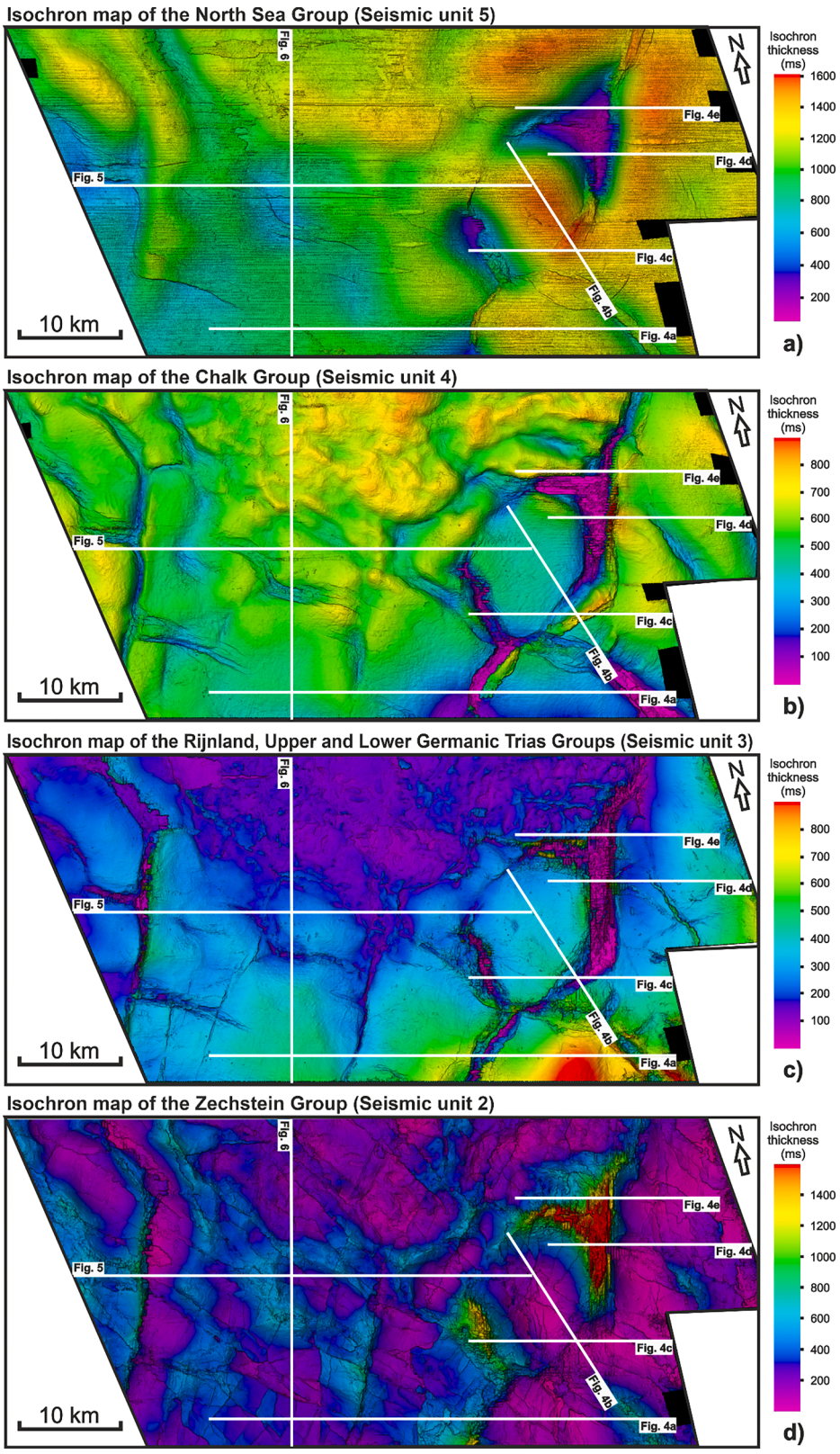

Fig. 8. Isochron maps for four key seismic-stratigraphic units in the study area, including the North Sea Group (Seismic unit 5), Chalk Group (Seismic unit 4), Rijnland, Upper and Lower Germanic Trias Groups (Seismic unit 3) and Zechstein Group (Seismic unit 2), respectively. (a-c) Maps showing the thickness variation in three supra-salt stratigraphic units, marking the thinning of strata towards salt structures. (d) Map highlighting the thickness variation in the Zechstein salt, and the distribution of salt structures. The location of the seismic profiles in Figs. 4–6 is shown by the white lines.

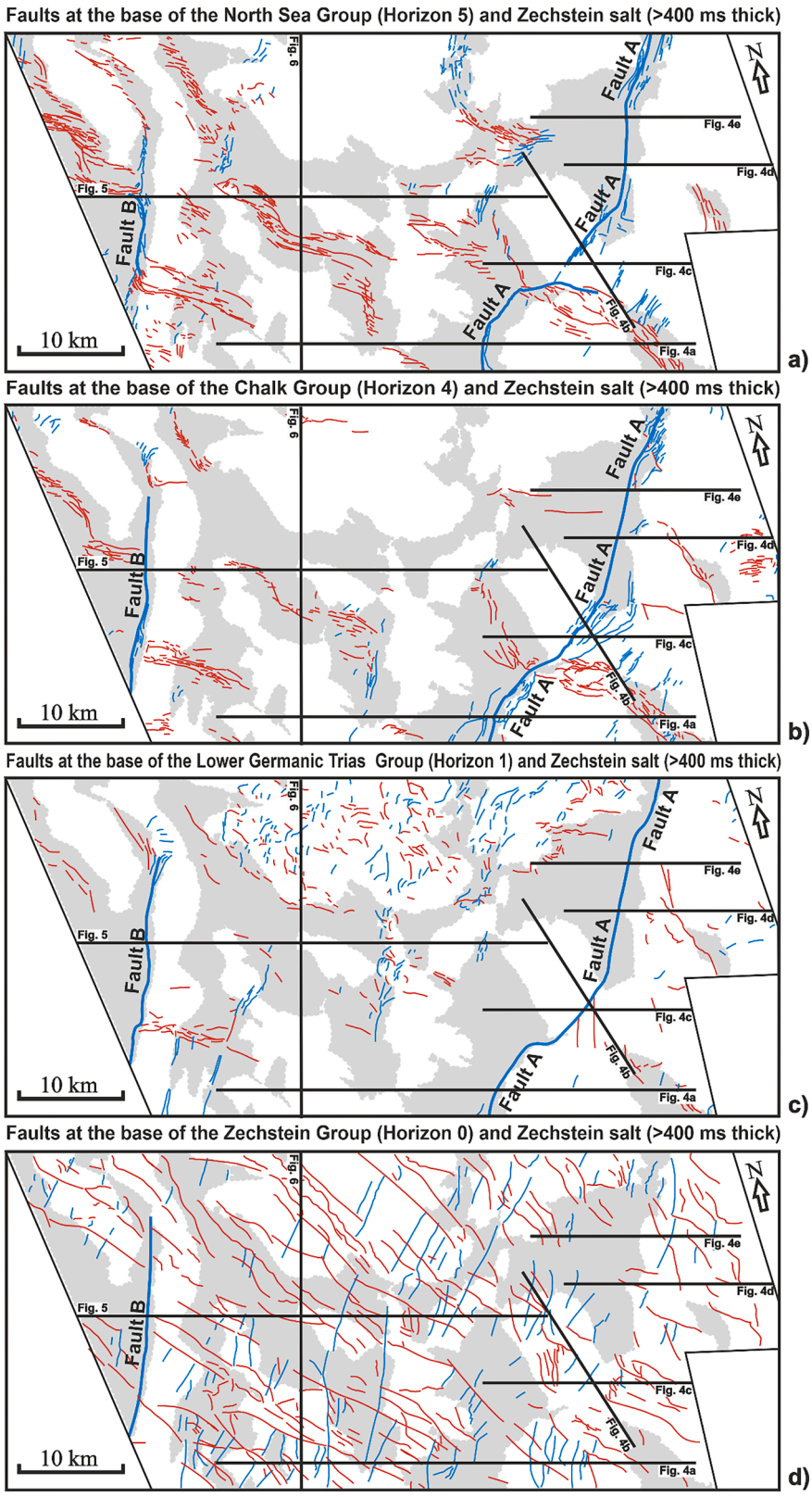

Fig. 9. Fault maps at four key horizons superimposed on the areas of the Zechstein salt (>400 ms thick), including the base of the North Sea Group (Horizon H5), Chalk Group (Horizon H4), Lower Germanic Trias Group (Horizon H1) and Zechstein Group (Horizon H0), respectively. (a-c) Maps with the distribution of supra-salt faults, highlighting that thick Zechstein salt controls the formation and development of supra-salt faults. Additionally, large supra-salt and hard-linked faults bound the thick Zechstein salt. (d) Map with the distribution of sub-salt faults, highlighting the control of sub-salt faults on the position and distribution of overlying salt structures. NW-striking faults are shown by thin red lines. NE-striking faults are shown by thin blue lines, except for Fault A and B marked by thick blue lines. The location of the seismic profiles in Figs. 4–6 is shown by black lines.

In contrast, polygonal faults are usually developed away from salt structures, formed by the volumetric contraction of very fine-grained sediments compacting and dewatering during the initial burial phases of strata (Cartwright and Lonergan, 1996; Cartwright et al., 2003). The length of polygonal faults varies from 200 to 1500 m, and their maximum displacements range from 25 to 60 m. Although faults are abundant in the North Sea Group, they are developed in strata placed at a depth shallower than ~1670 ms twtt (Figs. 4–7).

A few large supra-salt faults offset the strata above the Zechstein Group. They detach on the top of the Zechstein Group evaporites and may even propagate into these latter (Figs. 4–7). These large supra-salt faults are mainly NE- and NW-striking, the largest of which are NE-striking and formed due to NW-SE Mesozoic extension (Fig. 9a-c). They have also experienced multiple phases of activity during the Mesozoic and Cenozoic (Figs. 4 and 5). The larger NE-striking faults are mainly located along the boundary of thick salt intervals (>400 ms) (Fig. 9). For example, Fault A bounds two large salt diapirs (Figs. 7 and 9), and its measured length is 36,678 m, for a maximum displacement of 1647 m. Comparatively, NW-striking supra-salt faults are usually developed above salt structures, locally showing en echelon arrangement (Fig. 9). They are mainly crestal faults whose formation is associated with the growth of salt structures. The largest NW-striking fault has the length of 10,600 m, and its maximum displacement reaches to 391 m. In parallel, there is also a cluster of small supra-salt faults with random strikes developed above thin salt (<400 ms) in the northern sector of the study area (Figs. 6, 7 and 9). These faults were likely formed due to salt movement during the Early Jurassic, as they have small throws and show local thickening of strata on their immediate hanging-walls, at the level of horizon H1 (Fig. 6).

5.2.2. *Sub-salt faults*

Sub-salt faults are well developed on the Cleaver Bank High, striking to the NW and NE (Figs. 4–7 and 9). They are usually longer than supra-salt faults, with lengths varying from 0.7 to 15.8 km (Figs. 7 and 9). NE-striking faults intersect NW-striking faults, forming rhomboid or rectangular shapes in plan view. Many of these sub-salt faults bound the area where thick (>400 ms) Zechstein salt is observed, and their strikes are similar to those of overlying salt structures (Figs. 7–9). This implies that sub-salt faults controlled the position and distribution of salt structures in the study area.

In seismic data, sub-salt faults are usually steep and with relatively small throws (Figs. 4–6). They were mainly formed in the Upper Palaeozoic, and likely inherited from pre-existing weakness zones in the paleozoic basement (Ziegler, 1990; Schroot and Haan, 2003). These faults have experienced multiple phases of reactivation, resulting in their high length-throw ratios (Ligtenberg et al., 2011; Van Ojik et al., 2020; Alves et al., 2022).

5.2.3. *Hard-linked faults*

There are only a few hard-linked faults in the study area, and most of them show a prevalent NE strike (Figs. 5, 7 and 9). This can be explained by the Mesozoic reactivation of NE-striking sub-salt faults, which caused

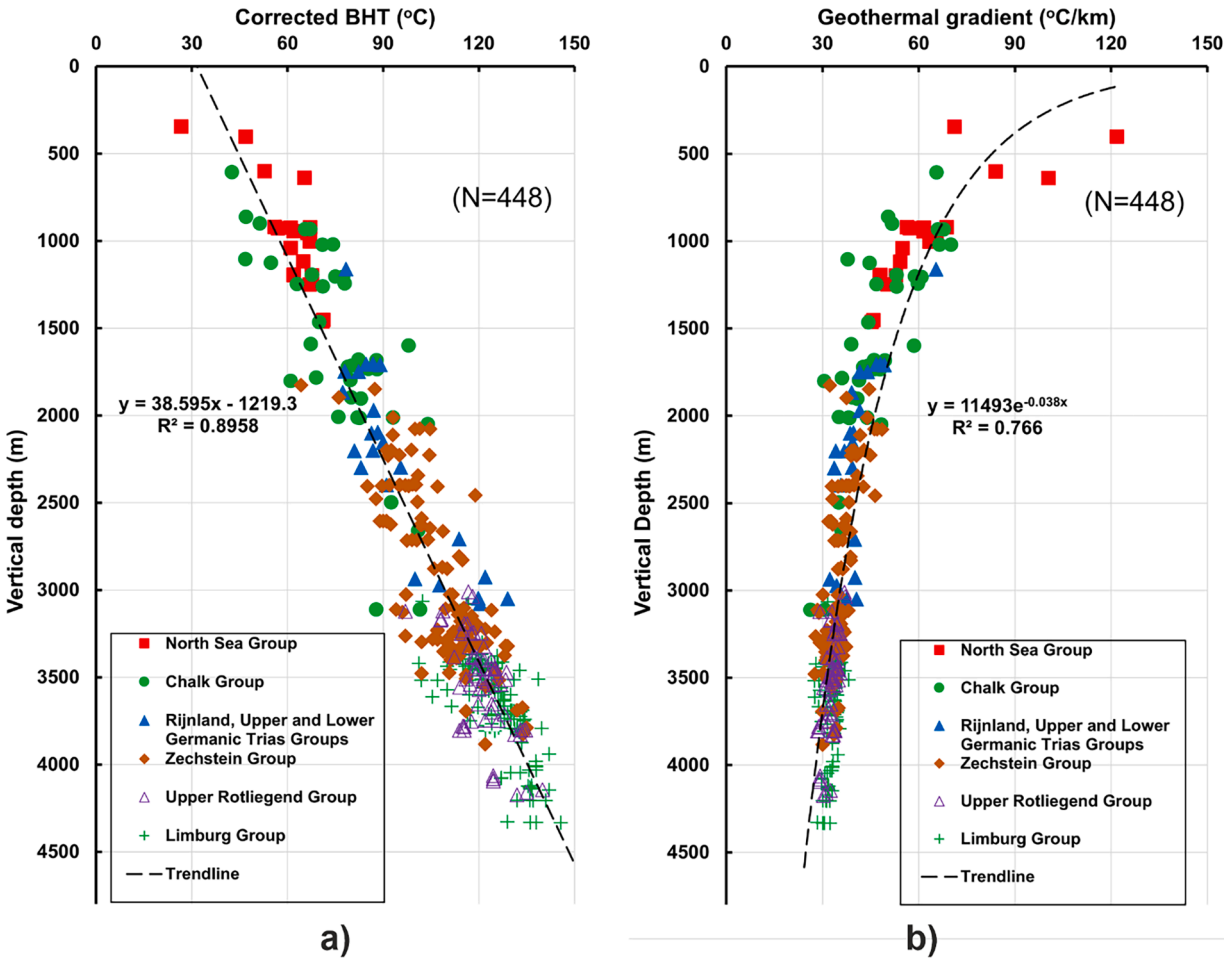

Fig. 10. (a) Corrected BHT in five seismic-stratigraphic units as recorded from the 48 exploration wells analysed in the study area. The trendline of all (448) corrected BHTs (See Supplementary File 1) shows a near-linear positive correlation with depth, with an average geothermal gradient of 38.54°C/km. (b) Geothermal gradient calculated from all (448) corrected BHTs in five seismic-stratigraphic units in the study area. The trendline of all (448) geothermal gradients shows a near-exponential decreasing trend in geothermal gradient with depth.

them to propagate across the Zechstein Group to form hard-linked structures. The largest hard-linked fault (Fault B) is located in the western sector of the study area, and it is a large NE-striking dextral strike-slip fault with a length of 19.4 km (Figs. 5, 7 and 9). Lateral offset in Fault B reaches a maximum of ~9.1 km based on the distance between two equivalent NW-striking faults that were offset by it (Figs. 7–9). In addition, Fault B is nearly vertical and propagated from the sub-salt Rotliegend Group into the relatively shallow supra-salt North Sea Group (Fig. 5).

6. Subsurface temperature and geothermal gradients

BHT data reveal corrected temperatures ranging from 26.6°C to 145.7°C, with a near-linear positive correlation with depth (Fig. 10a). The temperature trendline in Fig. 10a shows a gradient of 38.5°C/km. In contrast, geothermal gradients vary from 26.3°C/km to 121.8°C/km, highlighting a negative correlation with depth that follows an exponential relationship (Fig. 10b). The lowest figure (P90), median (P50) and the highest figure (P10) of corrected BHTs and geothermal gradients vary in different stratigraphic units (Table 1). The P90, P50 and P10 BHTs of supra-salt strata are higher than those in the Zechstein Group and sub-salt strata (Table 1). Conversely, the P90, P50 and P10 of geothermal gradients in supra-salt strata are much lower than those in the Zechstein Group and sub-salt strata (Table 1).

The Limburg Group records the highest P90, P50 and P10 BHTs, respectively 114.6°C, 125.3°C and 135.9°C (Table 1). The Upper Rotliegend Group has the second highest P90, P50 and P10 BHTs, which are respectively 112.6°C, 121.7°C and 130.9°C. In contrast, the North Sea and Chalk Groups have the lowest P90, P50 and P10 BHTs (Table 1). The P90, P50 and P10 BHTs of the Zechstein Group (Seismic Unit 2) are slightly higher than in the Rijnland, Upper and Lower Trias and Groups (Seismic Unit 3). In terms of geothermal gradients, the North Sea and Chalk Groups record the highest P90, P50 and P10 values for geothermal gradients (Table 1). The Upper Rotliegend and Limburg Groups have the lowest P90, P50 and P10 values for geothermal gradients, averaging 33°C/km. The P90, P50 and P10 values for geothermal gradients are very similar for the Zechstein Group (Seismic Unit 2) and Rijnland, Upper and Lower Trias and Groups (Seismic Unit 3), averaging 38°C/km.

Temperature maps from four (4) key horizons, superimposed on the areas of Zechstein Group (>400 ms thick), illustrate the recorded variations in subsurface temperatures (Fig. 11). They show the temperature at the base of the North Sea Group (Seismic Unit 5) ranging from 40 to 82°C, with low-temperature zones mostly located in the western sector of the study area. Zones with relatively high temperatures occur in the northern and eastern sectors (Fig. 11a). Temperatures at the base of the Chalk Group vary from 74 to 117°C, with low-temperature zones in the northeast, northwest and south of the study area (Fig. 11b). Similarly to the base of the North Sea Group, high-temperature zones are located to the north, southeast and southwest. The data in Figs. 11a and 11b also show that temperature distribution at the base of the Chalk (Seismic Unit 4) and North Sea (Seismic Unit 5) groups does not correlate with the presence of thick salt (>400 ms) below. In turn, at the base of the Zechstein Group (Seismic Unit 2) and Rijnland, Upper and Lower Germanic Trias Groups (Seismic Unit 3), temperatures show a good match with the relative distribution of Zechstein salt (Fig. 11c and d). Zones with thick Zechstein salt (>400 ms) record lower temperatures when compared to zones with less than 400 ms of salt. Hence, BHTs at the base of the Rijnland, Upper and Lower Germanic Trias Groups (Seismic Unit 3) vary from 65 to 128°C, while BHTs at the base of the Zechstein Group (Seismic Unit 2) range from 95 to 135°C (Fig. 11c and d).

7. Burial and thermal histories of the Cleaver Bank High

The burial history of the Cleaver Bank High is similar to other structural highs in the vicinity (e.g. De Jager, 2003, 2007; Fattah et al., 2012). Burial history models for three selected wells highlight two main phases of subsidence and sedimentation during the Early Triassic-Middle Jurassic (~250–175 Ma) and Early Cretaceous-Holocene (~137–0 Ma), which led to the burial maximum recorded in the study area at present (Fig. 12a,c and e). In parallel, multiple phases of uplift and erosion occurred during the Late Carboniferous-Early Permian (~307–264 Ma) and Mid-Late Jurassic (~170–150 Ma), the latter of which is associated with the Mid-Late Kimmerian phase (Fig. 12a, c and e). Two other phases of uplift are associated with tectonic inversion during the Late Cretaceous (Laramide phase) and Late Oligocene (Savian phase), but recording smaller magnitudes of uplift and erosion when compared to Mid-Late Jurassic uplift.

The thermal history for well K11–10 reveals two major temperature maxima occurring in the Early Cretaceous and Cenozoic (Fig. 12a). Pre-Zechstein units reached temperatures of up to 105°C during the Early Cretaceous, increasing to over 110°C during the Cenozoic. In contrast, wells K11–02 and K12–12 show one single temperature maximum during the Cenozoic (Fig. 12c and e). The highest modelled temperature for well K11–02 reaches 112°C, and is over 130°C in well K12-12. Importantly, modelled present-day temperatures in well K12–12 show a relatively good fit with the corrected BHTs analysed in this work (Fig. 12f). Temperature differences between modelled present-day temperatures and corrected BHTs for well K12-12 vary only from 0.6 to 12.4°C. Due to the thin salt encountered in well K12-12, modelled temperatures above and below the Zechstein Group are not distinctly affected by any salt thermal effect. Comparatively, a marked thermal effect of salt is recorded in wells K11-10 and K11-02, which show obvious variations in geothermal gradients above and below the Zechstein Group – salt is relatively thick near these two wells. Nevertheless, modelled present-day temperatures in wells K11-10 and K11-02 do not fit well with their corresponding corrected BHTs (Fig. 12b and d), recording temperature differences of 20.1-33.2°C and 14.7-26.4°C, respectively. This implies that subsurface temperatures in wells K11-10 and K11-02 are influenced by other factors apart from salt-related thermal effects.

Vertical thermal conductivity for different stratigraphic units was also modelled for wells K11-10, K11-02 and K12-12 (Fig. 12b, d and f). Thermal conductivities in different stratigraphic units are mainly controlled by their lithology, although local temperatures can also cause some variability. In the pre-Zechstein units (Seismic Unit 1), thermal conductivity varies between 1.3 and 1.9 W/(mK), values that mainly depend on lithology. Thermal conductivity in the Zechstein Group (Seismic Unit 2) ranges from 1.0 to 5.4 W/(mK). Salt records the highest thermal conductivity which, in our models, slightly decreases with temperature (burial depth). In contrast, interbedded claystones in the Zechstein Group have the lowest thermal conductivities. As for the Rijnland, Upper and Lower Germanic Trias Groups (Seismic Unit 3), their thermal conductivities vary from 1.6 to 2.5 W/(mK), once again depending on lithology. Thermal conductivities for the Chalk (Seismic Unit 4) and North Sea Groups (Seismic Unit 5) vary between 1.8 and 2.5 W/(mK) and 1.5 to 2.5 W/(mK), respectively. They both show a slight increase in thermal conductivity with increasing temperature (burial depth).

8. Discussion

8.1. Influence of salt structures on geothermal potential

Geothermal gradients in the Zechstein Group and overlying strata show a positive correlation with salt thickness, indicating that higher geothermal gradients occur above salt structures, following local increases in salt thickness (Fig. 13). Conversely, geothermal gradients in sub-salt strata show a slightly negative correlation with the thickness of the Zechstein Group (Fig. 13). Negative correlations can be explained by a greater heat flow from sub-salt to supra-salt strata in the areas where salt is thicker. Interestingly, geothermal gradients record fluctuations in

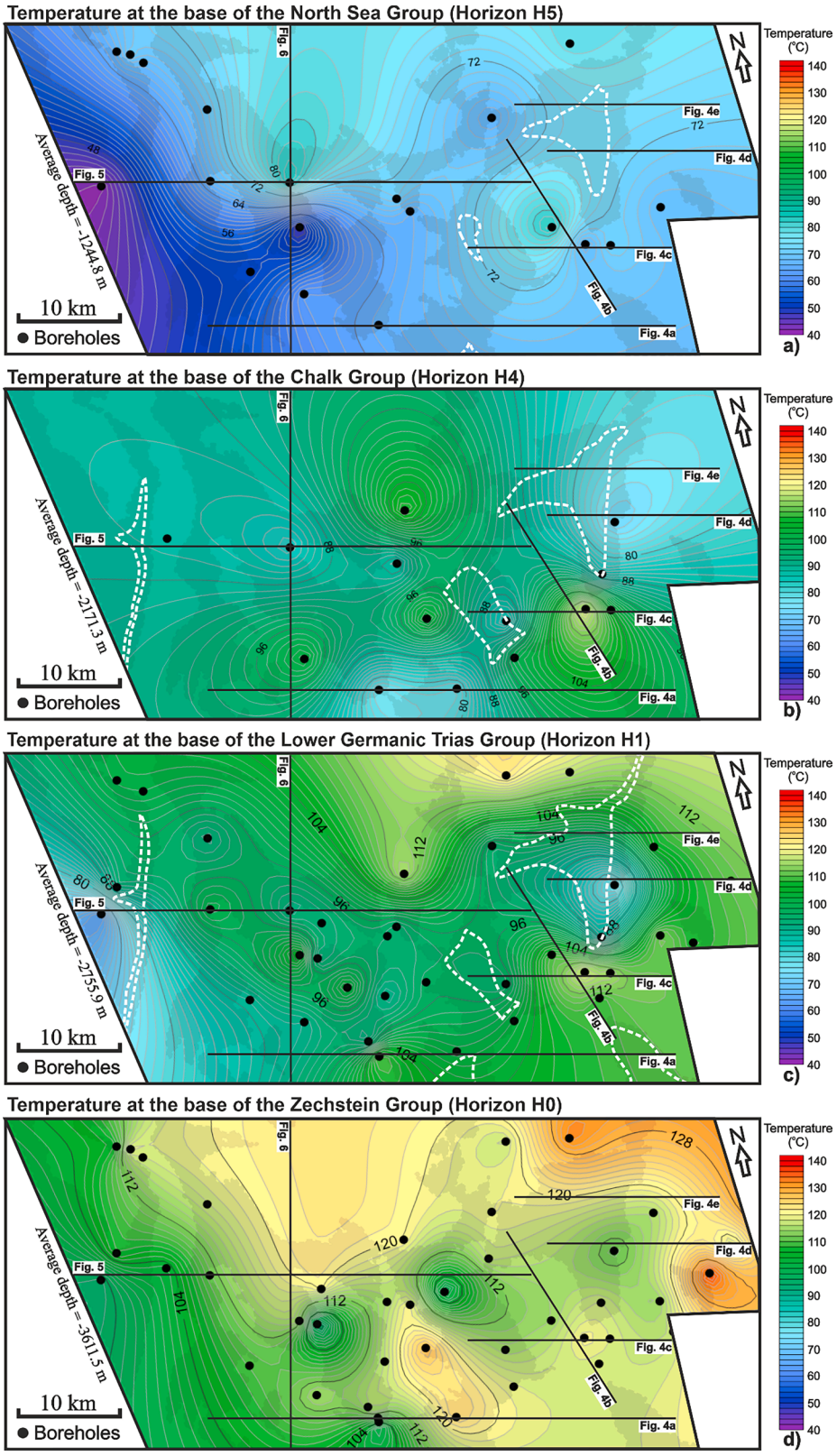

Fig. 11. Temperature maps superimposed on the areas of the Zechstein salt (>400 ms thick) at four key horizons, highlighting the subsurface temperature variations in the study area. a-d) Temperature at the base of the North Sea Group (Horizon H5), Chalk Group (Horizon H4), Lower Germanic Trias Group (Horizon H1) and Zechstein Group (Horizon H0), respectively. The Zechstein salt (>400 ms) is shown with the transparent black polygonal filling, and salt piercing boundaries in different horizons are marked by white dashed polygon. The position of borehole data used to compile these maps is marked by black circles, and their names are shown in Fig. 1c. The location of the seismic profiles in Figs. 4–6 is shown by the black lines.

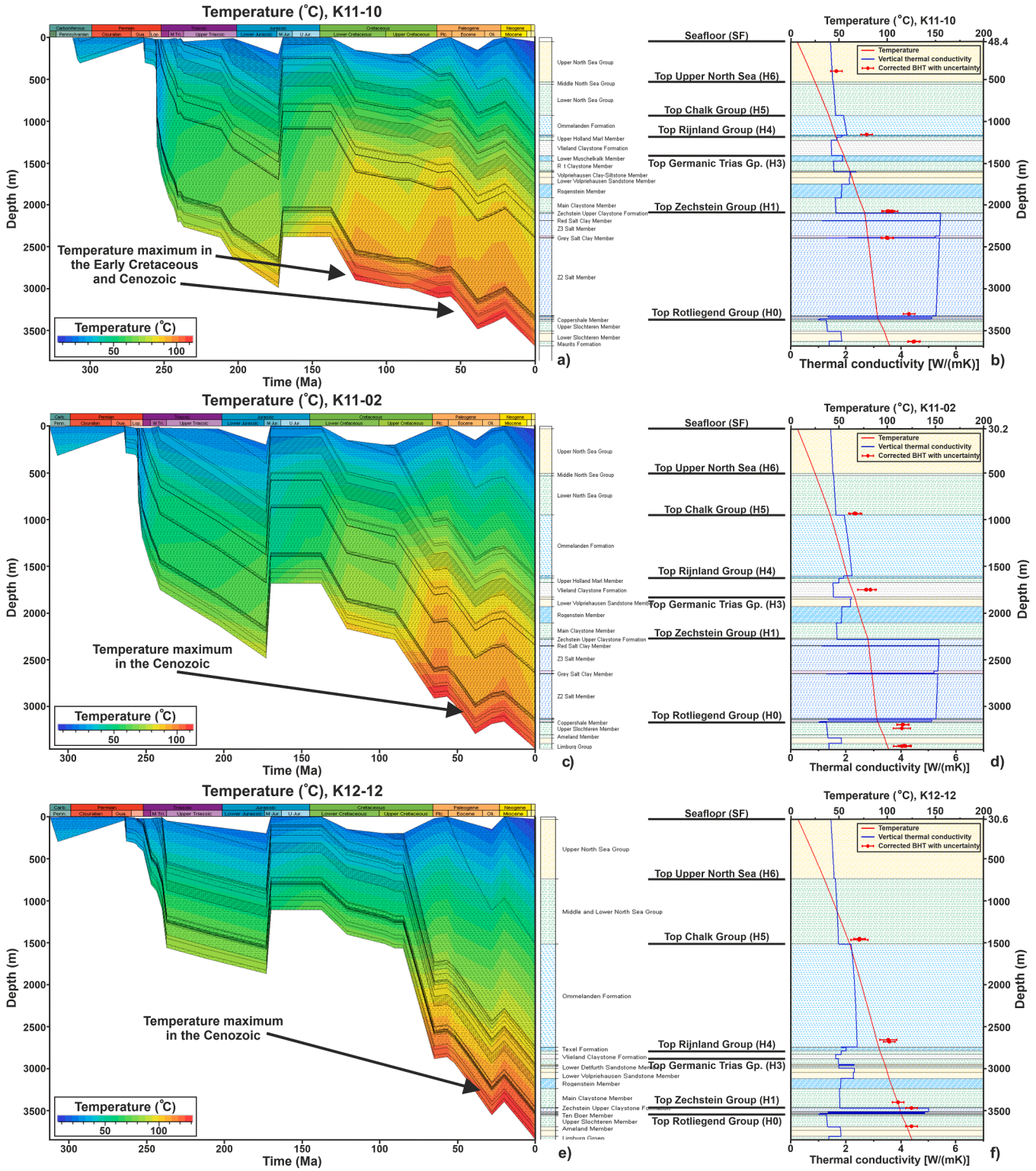

Fig. 12. Subsidence and thermal models for wells K11–10, K11–02 and K12–12, highlighting their modelled present-day temperatures, corrected BHTs and vertical thermal conductivities. The subsidence and thermal models provide evidence that temperature maximum occurred in the Early Cretaceous and Cenozoic. Temperature differences between modelled present-day temperatures and corrected BHTs for wells K11–10, K11–02 and K12–12 are respectively 20.1-33.2°C, 14.7-26.4°C and 0.6-12.4°C. This suggests that subsurface temperatures in wells K11–10 and K11–02 are influenced by other factors than the presence of nearby salt structures.

areas with a similar salt thickness, likely due to the differing burial depths of the salt structures interpreted on seismic. This is because salt thermal conductivity decreases with increasing temperature (Fig. 12b and d), resulting in higher geothermal gradients above salt structures that are relatively shallow (Raymond et al., 2022). Hence, if salt structures are deeper, the chimney effect of salt structures becomes less important due to its relatively lower salt thermal conductivity. In addition, the data in Fig. 13 show multiple outliers, implying that

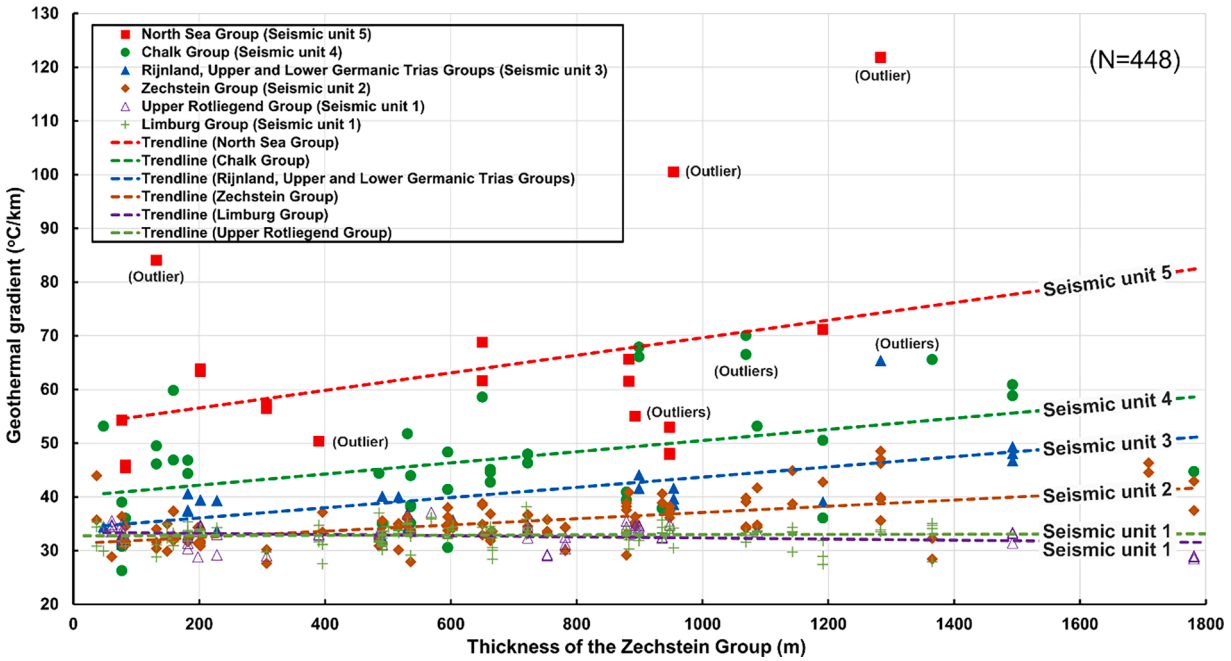

Fig. 13. Plot of geothermal gradient for different seismic-stratigraphic units vs. thickness of the Zechstein Group. Geothermal gradients in the North Sea Group (Seismic unit 5), Chalk Group (Seismic unit 4), Rijnland, Upper and Lower Germanic Trias Groups (Seismic unit 3) and Zechstein Group (Seismic unit 2) show a positive correlation with the thickness of the Zechstein Group. In contrast, geothermal gradients in the Upper Rotliegend and Limburg Groups show a negative correlation with the thickness of the Zechstein Group, a character explained by the presence of a greater heat flow from sub-salt to supra-salt strata in areas where salt is thicker.

subsurface geothermal gradients are influenced by other factors.

The effect of salt structures on geothermal potential can be observed on geothermal gradient maps (Fig. 14). Areas with thick Zechstein salt (>400 ms) correlate with relatively high geothermal gradients (> 49°C/km) in supra-salt strata (Fig. 14a). However, local geothermal gradients are influenced by large supra-salt faults, especially around Fault A. Similarly to supra-salt strata, areas with thick (>400 ms) Zechstein salt are well matched to the higher geothermal gradients (>37°C/km) in the Zechstein Group (Fig. 14b). Areas with thick Zechstein salt (>400 ms) correlate with low geothermal gradients (<32°C/km) in sub-salt strata (Fig. 14c).

It is important to stress the influence of the Chalk Group on geothermal gradients (Fig. 15). Geothermal gradients in the North Sea and Chalk groups show a negative correlation with the thickness of this latter stratigraphic unit (Fig. 15). This can be explained by the low permeability of the Chalk Group, which hinders heat transfer from underlying strata. Geothermal gradients in the Zechstein Group (Seismic Unit 2) and Rijnland, Upper and Lower Germanic Trias Groups (Seismic Unit 3) also show a negative correlation with the thickness of the Chalk Group (Seismic Unit 4). In contrast, geothermal gradients in the Upper Rotliegend and Limburg Groups (Seismic Unit 1) do not show significant changes relative to the thickness of the Chalk Group (Fig. 15). Geothermal gradients in the two former units are not influenced by the Chalk Group, as they are buried much below. In parallel, geothermal gradients in shallow strata of the study area are also highly likely to be affected by the palaeoclimate, especially the last glaciation periods (e.g. Fuchs et al., 2015). This impact has been quantified by Fuchs et al. (2015) at the Hannover within the Southern Permian Basin using petrophysical well logs, not far from the study area, at a similar latitude. The authors indicated that geothermal gradient perturbations caused by palaeoclimatic impact can reach 10–12°C/km from the surface down to ~400 m, with such a geothermal gradient perturbation reduced to less than 5°C/km below ~800 m (Fuchs et al., 2015). This implies that the temperature and geothermal gradients measured in shallow strata, in this work, could have been even higher without the palaeoclimatic impact of past glaciations.

8.2. *The role of faults in influencing geothermal potential*

Faults controlled the geometry, position and spatial distribution of salt structures on the Cleaver Bank High (Figs. 7 and 9). Anomalies in geothermal gradient are recorded close to faults as documented in Tables 2 and 3.

8.2.1. *Direct influence of faults on geothermal potential*

A direct influence on geothermal potential occurs when focused fluid migration occurs along faults, when these faults act as effective paths to deep and hot fluid (Fig. 16). This leads to higher-than-expected geothermal gradients in shallow strata. However, the direct influence of faults on geothermal potential is usually limited to the areas adjacent to these structures. Their influence merely lasts for short periods, if no new hot fluid is transmitted through faults, as heat can be quickly rebalanced (Pruess, 2005, 2008; Li et al., 2018). The direct influence of faults on geothermal gradients is introduced below by using Fault A as an example.

Fault A is a growth fault propagating upwards from the Zechstein Group into the Upper North Sea Group (Fig. 4). It was formed during the Early Triassic, as shown by the thickening of the Upper and Lower Germanic Trias Groups on its hanging-wall block (Fig. 4a). It is also a part of a large NE-striking fault zone across the Southern North Sea (See Fig. 1 in Ten Veen et al., 2012). In supra-salt strata, geothermal gradients on the footwall of Fault A are much higher than on its immediate hanging-wall block (Table 2). Average geothermal gradients on the footwalls of Fault A are respectively 105%, 26% and 41% in the North Sea Group (Seismic Unit 5), Chalk Group (Seismic Unit 4) and Rijnland, Upper and Lower Germanic Trias Groups (Seismic Unit 3), values that are higher than on its immediate hanging-wall block (Table 2). In more detail, geothermal gradients recorded in well K11–10 - located on the footwall of Fault A - are the highest in all supra-salt strata, excluding the Chalk Group due to the lack of BHT data for this interval, which are respectively 121.8°C/km in the North Sea Group (Seismic Unit 5), 65.4°C/km in the Rijnland, Upper and Lower Germanic Trias Groups (Seismic Unit 3) and 48.5°C/km in the Zechstein Group (Seismic Unit 2)

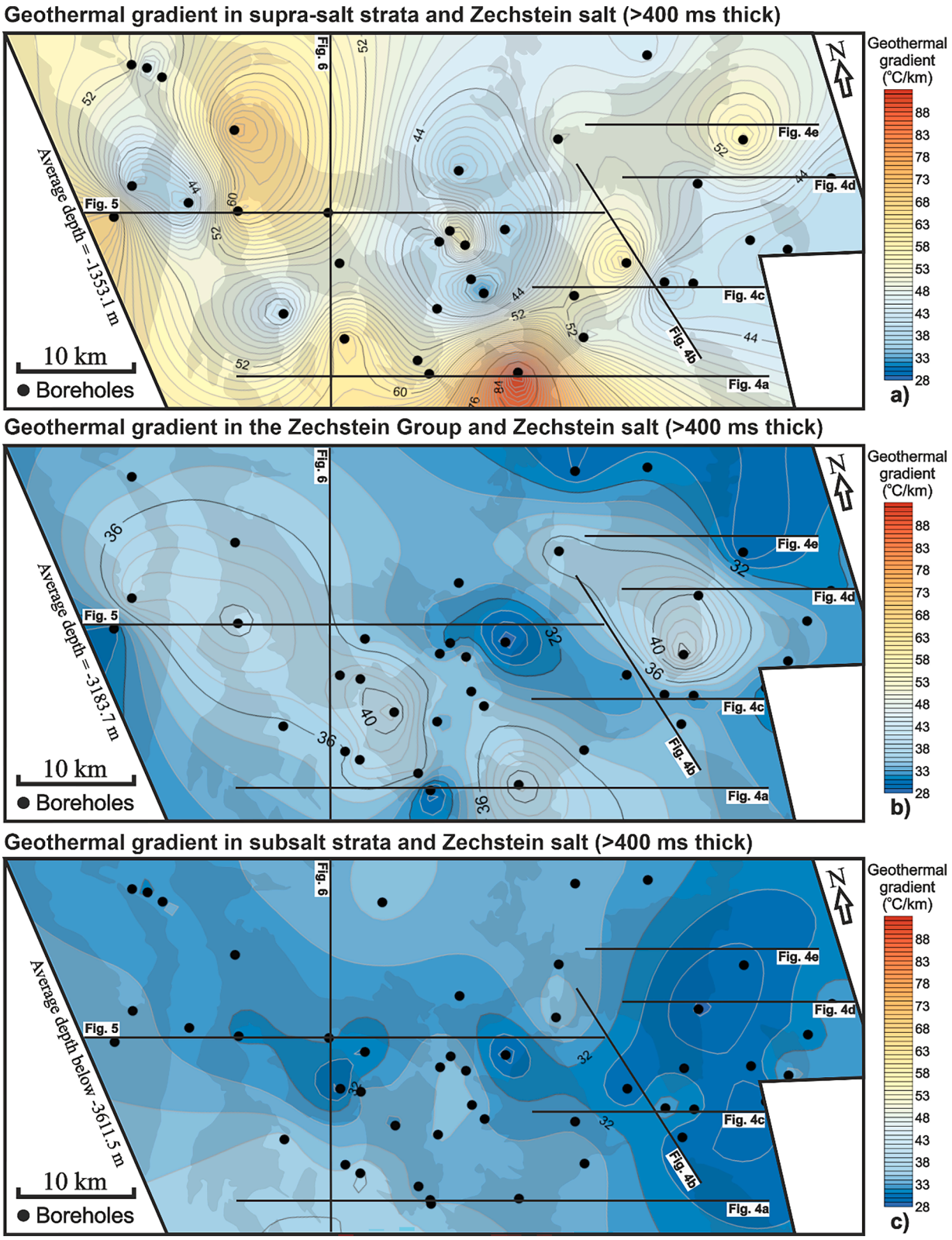

Fig. 14. Geothermal gradient maps for supra-salt strata, Zechstein Group and sub-salt strata superimposed on the areas with Zechstein salt (>400 ms thick). (a) and (b) Maps showing that areas with thick Zechstein salt (>400 ms thick) correlate with relatively high geothermal gradients. (c) Map highlighting that areas with the thick Zechstein salt (>400 ms thick) relate to areas of low geothermal gradients. The Zechstein salt (>400 ms thick) is shown with a transparent black polygonal filling. The position of borehole data used to compile these maps is marked by the black circles, and their names are shown in Fig. 1c). The location of the seismic profiles in Figs. 4–6 is shown by the black lines.

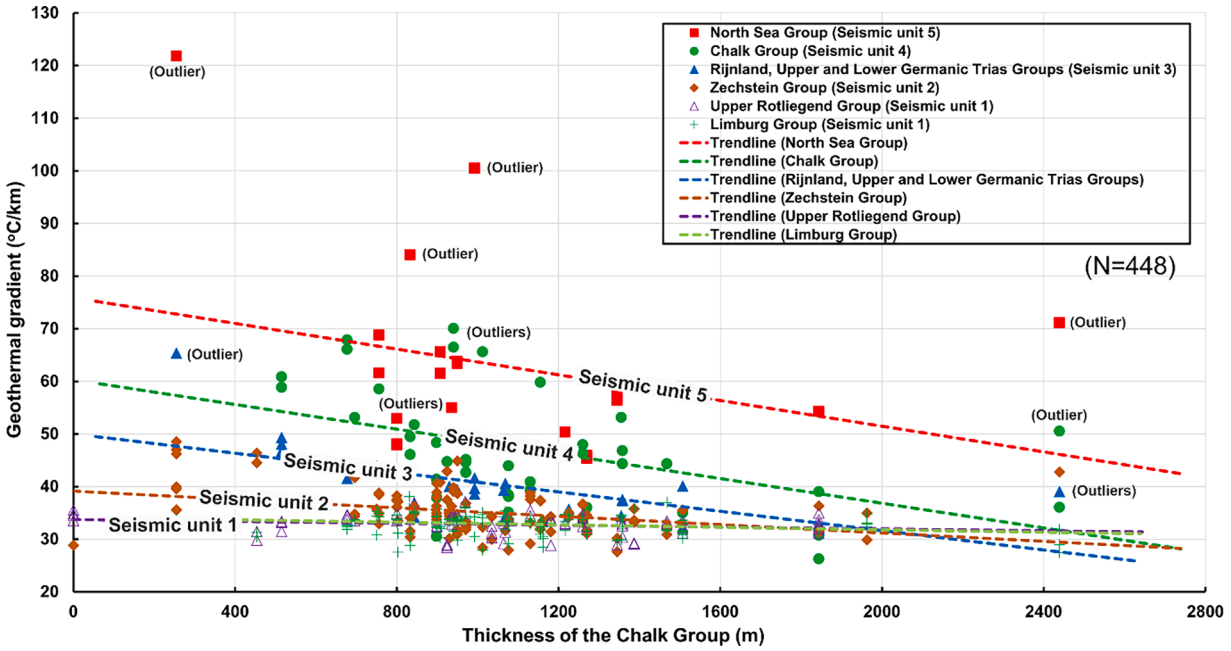

Fig. 15. Plot of geothermal gradient for different seismic-stratigraphic units vs. thickness of the Chalk Group. Geothermal gradients in the North Sea Group (Seismic unit 5), Chalk Group (Seismic unit 4), Rijnland, Upper and Lower Germanic Trias Groups (Seismic unit 3) and Zechstein Group (Seismic unit 2) show a negative correlation with the thickness of the Chalk Group. This can be explained by the low permeability of the Chalk Group, hindering the transfer of heat from underlying strata. Conversely, geothermal gradients in the Upper Rotliegend and Limburg Groups do not correlate with the thickness of the Chalk Group.

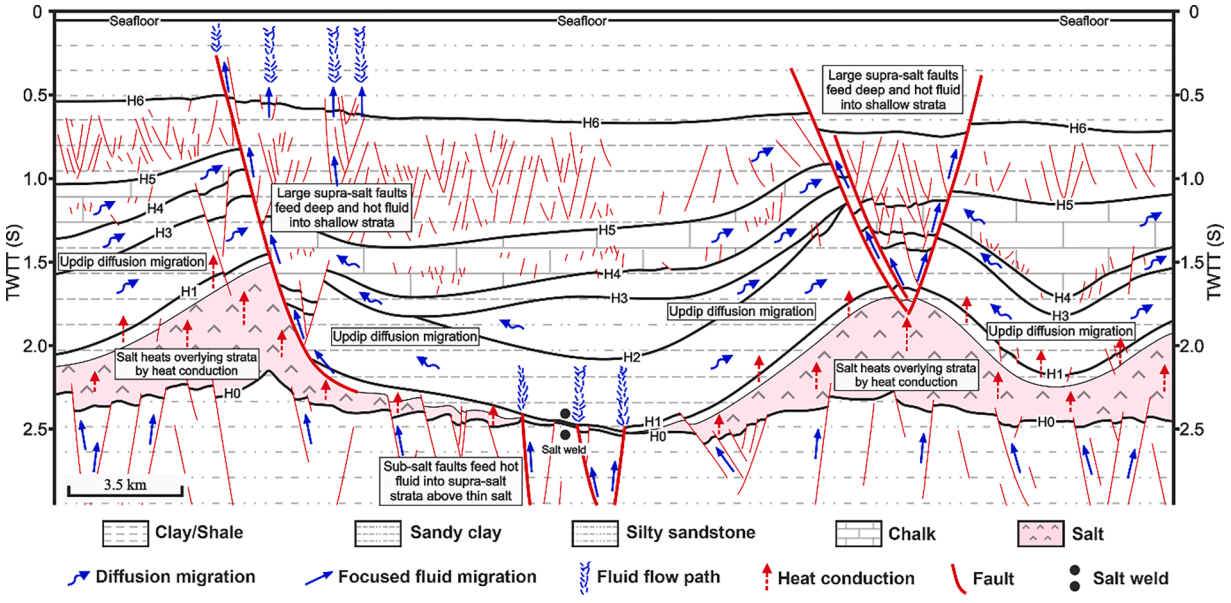

Fig. 16. Diagram summarising the influence of salt structures and faults on geothermal potential, highlighting three potential geothermal exploration targets in the study area. The Zechstein salt heats the overlying strata by heat conduction, causing higher geothermal gradients above salt strata. Large supra-salt and sub-salt faults act as fluid paths to deep and hot fluid into shallow strata, resulting in the presence of the high geothermal gradients in shallow strata. Three potential geothermal exploration targets are located at the footwall of a large supra-salt fault, above thick Zechstein salt, or in areas with salt welds and dense sub-salt faults. This section is modified from Figs. 4a and 6.

(Fig. 4a; Table 2). Comparatively, geothermal gradients recorded in wells K11-08 and K12-12, i.e. on the hanging-wall block of Fault A, approach the lowest values in each of the supra-salt units considered in this work (Table 2).

Such an observation suggests the footwalls of large supra-salt faults to be favourable geothermal exploration targets, a character justified by the fact that salt in these footwalls is also thicker when compared to their hanging-wall blocks (Fig. 4; Table 2). Thicker salt is likely to cause 'chimney effects' near the largest faults. More importantly, it is related to fluid migration along Fault A into shallow strata, as multiple low-amplitude trails of fluid are observed in the hanging-wall of Fault A in Fig. 4a. This can also be confirmed by the distinct differences between modelled present-day temperatures and corrected BHTs for wells K11–10 and K11–02 that are located on the footwall of Fault A, as their corrected BHTs are much higher than their modelled present-day temperatures (Fig. 12b and d). In contrast, modelled well K12–12 that is

located on the hanging wall of Fault A is almost free of perturbations caused by salt structures and faults, showing that its corrected BHTs relatively fit well with modelled present-day temperatures (Fig. 12f). In addition, depth differences between the footwall of large supra-salt faults and their corresponding hanging-wall can also partly account for this observation, as geothermal gradient has a negative correlation with depth (Fig. 10b). Footwalls are also effective structural traps for fluid, so the fluid accumulated by diffusion and focused fluid migrations are more likely to be preserved in the footwalls of faults (Fig. 16). This has already been proven by the hydrocarbon accumulations thus far encountered near some of the wells drilled in the study area.

The relative distance from the largest faults influences the geothermal gradients recorded in supra-salt strata (Fig. 4; Table 2). Geothermal gradient in the Rijnland, Upper and Lower Germanic Trias Groups (Seismic Unit 3) gathered from well K11–10 is 65.4°C/km, a higher value than the 44.1°C/km recorded in well K11–02 (Fig. 4a; Table 2). These two wells are located on the footwall of Fault A, but well K11–10 is located much closer to this fault (Fig. 4a; Table 2). This explains why the difference between modelled present-day temperatures and corrected BHTs is larger for well K11–10 than for well K11–02 (Fig. 12b and d). These data prove that large supra-salt faults significantly increase the local geothermal gradients in their vicinity, but their influence decreases as one moves away from them. Furthermore, large NW-striking crestal faults can influence the geothermal gradients around salt structures (Figs. 6 and 16; Table 3). These faults propagate into the Upper North Sea Group from the Zechstein Group (Figs. 6, 7 and 9), and high geothermal gradients are recorded next to these faults (Table 3). In detail, the second highest geothermal gradient (100.5°C/km), recorded in well K07–01 within the North Sea Group, is located next to the crestal faults in Fig. 6 (also see Table 3). The presence of this high geothermal gradient is high likely be associated with the influence of these crestal faults, though the underlying thick salt may have also contributed in part (Figs. 13 and 16).

Sub-salt faults impose a direct influence on the geothermal potential of the Cleaver Bank High. This usually occurs in the areas where the Zechstein salt is very thin (<100 ms; or ~230 m), or even absent, promoting fluid flow along sub-salt faults into supra-salt strata (Fig. 4c-e and 16). As a key example, well K09–03 was drilled next to a low-amplitude trail of fluid located above a salt weld (Fig. 4c). A relatively high geothermal gradient (40.6°C/km) is recorded in well K09–03 within the Rijnland, Upper and Lower Germanic Trias Groups (Seismic Unit 3; Table 3), suggesting fluid flow into supra-salt strata. The presence, near this well, of a relatively high geothermal gradient implies very recent, if not active, fluid flow.

8.2.2. *Indirect influence of faults on geothermal potential*

An indirect influence of faults on geothermal potential is recorded where higher geothermal gradients occur in supra-salt strata, but lower geothermal gradients are observed in sub-salt strata (Figs. 13, 14 and 16). In the study area, faults control the geometry, position and spatial pattern of salt structures, showing they have an indirect influence on the Cleaver Bank's geothermal potential.

Supra-salt faults are the most common faults in the study area, but most are restricted to Cenozoic strata. Only a few large Mesozoic supra-salt faults propagated upward into the North Sea Group (Figs. 4–6). These large supra-salt faults exerted an effective control on the geometry of salt structures, but not on their spatial distribution (Fig. 9). Sub-salt faults are mainly NW- or NE-striking in the study area and experienced multiple episodes of reactivation. They control the strike and thickness of salt structures, creating the necessary accommodation space on their hanging-wall blocks for thick Zechstein salt (Fig. 9). In parallel, large hard-linked faults can influence the distribution of salt structures. In the study area, a large strike-slip fault (Fault B) located in the western sector of the study area resulted in the formation of a ~20 km long salt wall (Fig. 5). The thickness of Zechstein salt changes on both sides of Fault B, generating contrasting geothermal gradients in supra-salt strata (Figs. 5 and 14; Table 3). These exert large-scale and long-lasting controls on geothermal gradients and subsurface temperatures when compared with the direct influence of faults on geothermal potential.

On the Cleaver Bank High, the greatest geothermal energy potential occurs at the footwall of large supra-salt faults, especially near Fault A. The area near such faults records high geothermal gradients due to the combined presence of thick Zechstein salt at depth and the migration of hot fluid along these same faults. Another potential geothermal exploration target is located above thick salt intervals in the Zechstein Group, as thick salt can heat supra-salt strata up due to its good thermal conductivity. The last potential geothermal exploration target in the Cleaver Bank High coincides with the sector where thin salt (<100 ms) is observed above dense sub-salt faults. Here, sub-salt fluid can flow upwards along the sub-salt faults, resulting in the migration of deep and hot fluid across salt welds.

9. Conclusions

This work aimed at understanding the influence of salt structures and faults on the geothermal potential of the Cleaver Bank High, Southern North Sea. Salt structures and faults were analysed, and subsurface temperature and geothermal gradient maps were compiled. The influence of salt structures and faults on the geothermal potential of the study area was discussed. The main conclusions of this work can be summarised as follows:

(a) Salt structures developed on the Cleaver Bank High include multiple salt diapirs, salt pillows and a salt wall, all of which have experienced multiple phases of growth. Their relative positions, geometries and distributions are significantly controlled by sub-salt faults and large NE-striking supra-salt faults.
(b) The presence of salt structures has an important influence on the geothermal potential of the study area. In more detail, strata deposited above the Zechstein Group show higher geothermal gradients proportionally to the thickness of Zechstein salt. In contrast, the strata buried below this Group show a minor decreasing trend in geothermal gradients with an increasing thickness of salt. This proves the large-scale, long-lasting influence of salt on geothermal gradients and sub-surface temperatures.
(c) Faults developed on the Cleaver Bank High also play an important role in influencing the geothermal potential. Large supra-salt faults can act as migration paths for deep and hot fluid, resulting in the presence of the high geothermal gradients in shallow strata. Geothermal gradients on footwall blocks are usually higher than that on the corresponding hanging-walls of large supra-salt faults. However, it decreases with the distance away from these faults, and their influence merely lasts for short periods, if no new hot fluid is transmitted through faults, as heat can be quickly rebalanced.
(d) Sub-salt faults influence the geothermal gradient of supra-salt strata in the sector where there is very thin, or even absent, salt (<100 ms), forming distinct low-amplitude trails of fluid above these same faults. They indirectly influence geothermal gradient by controlling the position, geometry and distribution pattern of salt structures.
(e) Faults and salt structures present a contrasting influence on temperatures and geothermal gradients. As a result, three potential geothermal exploration targets are summarised in the study area, located at the footwall of large supra-salt fault, above thick Zechstein salt, or areas with salt welds and dense sub-salt faults.

As a corollary, this work classifies the influence of tectonic faults on the geothermal potential of the Cleaver Bank High as: a) direct, and b) indirect. This highlights the contrasting influence of faults and salt

structures on geothermal gradients.

CRediT authorship contribution statement

Qiang Zhang: Conceptualization, Methodology, Formal analysis, Investigation, Writing – original draft, Visualization. **Tiago Alves:** Resources, Supervision, Writing – review & editing.

Declaration of Competing Interest

The authors declare that they have no known competing financial interests or personal relationships that could have appeared to influence the work reported in this paper.

Data availability

The authors do not have permission to share data.

Acknowledgments

The authors would like to acknowledge RockRose NL CS5 BV for permitting the use of 3D seismic volume and Dutch Oil and Gas portal (NLOG) for providing well data. We thank Gwen Pettigrew for helping our seismic data interpretation and for managing software licenses. The first author would like to acknowledge CSC (China Scholarship Council) for providing a PhD scholarship during his studies at Cardiff University. Schlumberger (Petrel® and PetroMod®) and Petroleum Experts (Move®) are acknowledged for the provision of the academic licences to Cardiff University's 3D Seismic Lab. We thank the editor-in-chief Christopher Bromley for his help, associate editor Gioia Falcone for his support and two anonymous reviewers for their constructive comments.

Supplementary materials

Supplementary material associated with this article can be found, in the online version, at doi:10.1016/j.geothermics.2023.102842.

References

Alberts, M.A., Underhill, J.R., Spencer, A., 1991. The effect of tertiary structuration on Permian gas prospectivity, Cleaver Bank Area, Southern North Sea, UK. In: Gener. Accum. Prod. Eur. Hydrocarb., 1, pp. 161–173. https://doi.org/10.1016/j.tecto.2014.07.015. European Association of Petroleum Geoscientists Special Publication, v.

Alves, T.M., Elliott, C., 2014. Fluid flow during early compartmentalisation of rafts: a North Sea analogue for divergent continental margins. Tectonophysics 634, 91–96. https://doi.org/10.1016/j.tecto.2014.07.015 vDOI.

Alves, T.M., Mattos, N.H., Newnes, S., Goodall, S., 2022. Analysis of a basement fault zone with geothermal potential in the Southern North Sea. Geothermics 102, 102398. https://doi.org/10.1016/j.geothermics.2022.102398 v.

Brown, A.R., 2001. Data polarity for the interpreter. Lead. Edge 20 (5), 549. https://doi.org/10.1190/1.1438994 v-549.

Busby, J., 2014, Geothermal energy in sedimentary basins in the UK: hydrogeology journal, v. 22, no. 1, p. 129–141. DOI: 10.1007/s10040-013-1054-4.

Canova, D.P., Fischer, M.P., Jayne, R.S., Pollyea, R.M., 2018. Advective heat transport and the salt chimney effect: a numerical analysis. Geofluids 2018. https://doi.org/10.1155/2018/2378710 v.

Cartwright, J., Lonergan, L., 1996. Volumetric contraction during the compaction of mudrocks: a mechanism for the development of regional-scale polygonal fault systems. Basin Res. 8 (2), 183–193. https://doi.org/10.1046/j.1365-2117.1996.01536.x v.

Cartwright, J., James, D., Bolton, A., 2003. The Genesis of Polygonal Fault Systems: A Review, 216. Geological Society, London, Special Publications, pp. 223–243. https://doi.org/10.1144/gsl.sp.2003.216.01.15. , v.

Chapman, D.S., Keho, T., Bauer, M.S., Picard, M.D., 1984. Heat flow in the Uinta Basin determined from bottom hole temperature (BHT) data. Geophysics 49 (4), 453–466. https://doi.org/10.1190/1.1441680 v.

Chen, P., 2016, Fault reactivation analysis of the Cleaver Bank High based on 3D seismic data.

Cloetingh, S., van Wees, J.D., Ziegler, P., Lenkey, L., Beekman, F., Tesauro, M., Förster, A., Norden, B., Kaban, M., Hardebol, N., 2010. Lithosphere tectonics and thermo-mechanical properties: an integrated modelling approach for enhanced geothermal systems exploration in Europe. Earth Sci. Rev. 102 (3–4), 159–206. https://doi.org/10.1016/j.earscirev.2010.05.003 v.

Corrigan, J., 1997, Correcting bottom hole temperature data, AEPT Research Memo RM 97-0007.

Corrigan, J. 2003, Correcting bottom hole temperature data. From https://www.zetaware.com/utilities/bht/default.html.

Daniilidis, A., Herber, R., 2017. Salt intrusions providing a new geothermal exploration target for higher energy recovery at shallower depths. Energy 118, 658–670. https://doi.org/10.1016/j.energy.2016.10.094 v.

De Jager, J., 2003. Inverted basins in the Netherlands, similarities and differences. Neth. J. Geosci. 82 (4), 339–349. https://doi.org/10.1017/S0016774600020175 v.

De, Jager, 2007. Geological development. Geol. Neth. 5, 26 v.

Deckers, J., van der Voet, E., 2018. A review on the structural styles of deformation during Late Cretaceous and Paleocene tectonic phases in the southern North Sea area. J. Geodyn. 115, 1–9. https://doi.org/10.1016/j.jog.2018.01.005 v.

Deckers, J., Rombaut, B., Broothaers, M., Dirix, K., Debacker, T., 2022. New 3D fault model for eastern Flanders (Belgium) providing insights on the major deformation phases in the region since the late Paleozoic. J. Struct. Geol., 104779 https://doi.org/10.1016/j.jsg.2022.104779.

Defant, A., 1961, Physical Oceanography, Pergamon.

Deming, D., 1989. Application of bottom-hole temperature corrections in geothermal studies. Geothermics 18 (5–6), 775–786. https://doi.org/10.1016/0375-6505(89)90106-5 v.

Doornenbal, H., Stevenson, A., 2010. Petroleum Geological Atlas of the Southern Permian Basin area. EAGE.

Erdlac Jr, R., Armour, L., Lee, R., Snyder, S., Sorensen, M., Matteucci, M., Horton, J., 2007. Ongoing resource assessment of geothermal energy from sedimentary basins in Texas. In: Proceedings of the Thirty-second Workshop on Geothermal Reservoir Engineering. Stanford University, Stanford, p. California.

Evans, T.R., Coleman, N., 1974. North Sea geothermal gradients. Nature 247 (5435), 28–30. https://doi.org/10.1038/247028a0 v.

Fattah, R.A., Verweij, J., Witmans, N., Ten Veen, J., 2012. Reconstruction of burial history, temperature, source rock maturity and hydrocarbon generation in the northwestern Dutch offshore. Neth. J. Geosci. 91 (4), 535–554. https://doi.org/10.1017/s0016774600000378 v.

Fuchs, S., Balling, N., Förster, A., 2015. Calculation of thermal conductivity, thermal diffusivity and specific heat capacity of sedimentary rocks using petrophysical well logs. Geophys. J. Int. 203 (3), 1977–2000. https://doi.org/10.1093/gji/ggv403.

Gallup, D.L., 2009. Production engineering in geothermal technology: a review. Geothermics 38 (3), 326–334. https://doi.org/10.1016/j.geothermics.2009.03.001 v.

Glaas, C., Genter, A., Girard, J., Patrier, P., Vidal, J., 2018. How do the geological and geophysical signatures of permeable fractures in granitic basement evolve after long periods of natural circulation? Insights from the Rittershoffen geothermal wells (France). Geotherm. Energy 6 (1), 1–25. https://doi.org/10.1186/s40517-018-0100-9 v.

Glennie, K., 1997. History of Exploration in the Southern North Sea: Geological Society, 123. Special Publications, London, pp. 5–16. https://doi.org/10.1144/gsl.sp.1997.123.01.02 v.

Harding, R., Huuse, M., 2015. Salt on the move: multi stage evolution of salt diapirs in the Netherlands North Sea. Mar. Pet. Geol. 61, 39–55. https://doi.org/10.1016/j.marpetgeo.2014.12.003 vDOI.

Hernandez, K., Mitchell, N.C., Huuse, M., 2018. Deriving Relationships Between Diapir Spacing and Salt-Layer Thickness in the Southern North Sea: Geological Society, 469. Special Publications, London, pp. 119–137. https://doi.org/10.1144/sp469.16 v.

Hinz, N.H., Faulds, J.E., Coolbaugh, M.F., 2014. Association of fault terminations with fluid flow in the Salt Wells geothermal field, Nevada, USA. Geotherm. Resour. Counc.Trans. 38, 3–10 v.

Holgate, F.L., 2005, Exploration and evaluation of the Australian geothermal resource.

Jackson, M.P., Hudec, M.R., 2017. Salt tectonics: Principles and Practice. Cambridge University Press.

James, D., 2003. The millennium atlas: petroleum geology of the central and northern North Sea. Geol. Mag. 140 (4), 487 v.

Jensen, P., 1983. Calculations on the thermal conditions around a salt diapir. Geophys. Prospect. 31 (3), 481–489. https://doi.org/10.1111/j.1365-2478.1983.tb01064.x v.

Jensen, P.K., 1990. Analysis of the temperature field around salt diapirs. Geothermics 19 (3), 273–283. https://doi.org/10.1016/0375-6505(90)90047-F v.

Li, W., Li, X., Peng, Y., Wang, Y., Tu, J., 2018. Experimental and numerical investigations on heat transfer in stratified subsurface materials. Appl. Therm. Eng. 135, 228–237. https://doi.org/10.1016/j.applthermaleng.2018.02.037 v.

Ligtenberg, H., Okkerman, J., and De Keijzer, M., 2011, Fractures in the Dutch Rotliegend—an overview. DOI: 10.2110/pec.11.98.0229.

McLean, K., McDowell, J., Sepulveda, F., Seastres, J., Zarrouk, S.J., Alcaraz, S., 2018. Upflow along a basement fault revealed by geothermal numerical pressure transient analysis. In: Proceedings of the 40th New Zealand Geothermal Workshop, 14, p. 16.

Mijnlieff, H.F., 2020. Introduction to the geothermal play and reservoir geology of the Netherlands. Neth. J. Geosci. https://doi.org/10.1017/njg.2020.2 v. 99. DOI.

Nolan, C., 2021, Geothermal energy and ice an unlikely alliance? Insights from temperature data on the Norwegian Continental Shelf.

Oudmayer, B., De Jager, J., 1993. Fault reactivation and oblique-slip in the Southern North Sea. In: Proceedings of the Geological Society, London, Petroleum Geology Conference Series, 4. The Geological Society of London, pp. 1281–1290. https://doi.org/10.1144/0041281.

Pruess, 2008. On CO2 fluid flow and heat transfer behavior in the subsurface, following leakage from a geologic storage reservoir. Environ. Geol. 54, 1677–1686. https://doi.org/10.1007/s00254-007-0945-x v.

Pruess, K., 2005. Numerical studies of fluid leakage from a geologic disposal reservoir for CO2 show self-limiting feedback between fluid flow and heat transfer. Geophys. Res. Lett. 32 (14) https://doi.org/10.1029/2005 gl023250 v.

Quirk, D., 1993. Interpreting the upper carboniferous of the dutch Cleaver Bank High. In: Proceedings of the Geological Society, London, Petroleum Geology Conference Series, 4. The Geological Society of London, pp. 697–706. https://doi.org/10.1144/0040697.

Raymond, J., Langevin, H., Comeau, F.A., Malo, M., 2022. Temperature dependence of rock salt thermal conductivity: implications for geothermal exploration. Renew. Energy 184, 26–35. https://doi.org/10.1016/j.renene.2021.11.080 v.

Reinecker, J., Hochschild, T., Kraml, M., Löschan, G., Kreuter, H., 2019. Experiences and challenges in geothermal exploration in the Upper Rhine Graben. In: Proceedings of the European Geothermal Congress, pp. 11–12.

Reinecker, J., Gutmanis, J., Foxford, A., Cotton, L., Dalby, C., Law, R., 2021. Geothermal exploration and reservoir modelling of the United Downs deep geothermal project, Cornwall (UK). Geothermics 97, 102226. https://doi.org/10.1016/j.geothermics.2021.102226 v.

Remmelts, G., 1995, Fault-related salt tectonics in the southern North Sea, the Netherlands. DOI: 10.1306/m65604c12.

Schroot, B.M., Haan, H.B.D., 2003. An Improved Regional Structural Model of the Upper Carboniferous of the Cleaver Bank High Based on 3D Seismic Interpretation: Geological Society, 212. Special Publications, London, pp. 23–37. https://doi.org/10.1144/GSL.SP.2003.212.01.03 v.

Stewart, S.A., Coward, M.P., 1995. Synthesis of salt tectonics in the southern North Sea, UK. Mar. Pet. Geol. 12 (5), 457–475. https://doi.org/10.1016/0264-8172(95)91502-g v.

Stewart, S.A., 2007. Salt Tectonics in the North Sea Basin: A Structural Style Template For Seismic interpreters: Geological Society, 272. Special Publications, London, pp. 361–396. https://doi.org/10.1144/GSL.SP.2007.272.01.19 v.

Ten Veen, J., Van Gessel, S., Den Dulk, M., 2012. Thin-and thick-skinned salt tectonics in the Netherlands; a quantitative approach. Neth. J. Geosci. 91 (4), 447–464. https://doi.org/10.1017/s0016774600000330 v.

Van Ojik, K., Silvius, A., Kremer, Y., Shipton, Z., 2020. Fault seal behaviour in Permian Rotliegend reservoir sequences. In: Case Studies from the Dutch Southern North Sea: Geological Society, 496. Special Publications, London, pp. 9–38. https://doi.org/10.1144/sp496-2018-189 v.

Van Wees, J.D., Stephenson, R., Ziegler, P., Bayer, U., McCann, T., Dadlez, R., Gaupp, R., Narkiewicz, M., Bitzer, F., Scheck, M., 2000. On the origin of the southern Permian Basin, Central Europe. Mar. Pet. Geol. 17 (1), 43–59. https://doi.org/10.1016/s0264-8172(99)00052-5 v.

Van Wees, J., Van Bergen, F., David, P., Nepveu, M., Beekman, F., Cloetingh, S., Bonté, D., 2009. Probabilistic tectonic heat flow modeling for basin maturation: assessment method and applications. Mar. Pet. Geol. 26 (4), 536–551. https://doi.org/10.1016/j.marpetgeo.2009.01.020 v.

Van Wees, J.D., Kronimus, A., Van Putten, M., Pluymaekers, M., Mijnlieff, H., Van Hooff, P., Obdam, A., Kramers, L., 2012. Geothermal aquifer performance assessment for direct heat production–methodology and application to Rotliegend aquifers. Neth. J. Geosci. 91 (4), 651–665. https://doi.org/10.1017/s0016774600000433 v.

Vidal, J., Genter, A., 2018. Overview of naturally permeable fractured reservoirs in the central and southern Upper Rhine Graben: insights from geothermal wells. Geothermics 74, 57–73. https://doi.org/10.1016/j.geothermics.2018.02.003 vDOI.

Wilson, A., Ruppel, C., 2007. Salt tectonics and shallow subseafloor fluid convection: models of coupled fluid-heat-salt transport. Geofluids 7 (4), 377–386. https://doi.org/10.1111/j.1468-8123.2007.00191.x v.

Wood, C.P., Brathwaite, R.L., Rosenberg, M.D., 2001. Basement structure, lithology and permeability at Kawerau and Ohaaki geothermal fields, New Zealand. Geothermics 30 (4), 461–481. https://doi.org/10.1016/s0375-6505(01)00003-7 v.

Yang, K., Huntington, J.F., Browne, P.R., Ma, C., 2000. An infrared spectral reflectance study of hydrothermal alteration minerals from the Te Mihi sector of the Wairakei geothermal system, New Zealand. Geothermics 29 (3), 377–392. https://doi.org/10.1016/s0375-6505(00)00004-3 v.

Younger, P.L., Gluyas, J.G., Stephens, W.E., 2012. Development of deep geothermal energy resources in the UK. In: Proceedings of the Institution of Civil Engineers-Energy, 165, pp. 19–32. https://doi.org/10.1680/ener.11.00009 v.

Zhang, Q., Alves, T., 2023. Palaeostress state around a rising salt diapir inferred from seismic reflection data. Mar. Pet. Geol. 155, 106385. https://doi.org/10.1016/j.marpetgeo.2023.106385.

Zhuo, Q., Meng, F., Zhao, M., Li, Y., Lu, X., Ni, P., 2016. The salt chimney effect: delay of thermal evolution of deep hydrocarbon source rocks due to high thermal conductivity of evaporites. Geofluids 16 (3), 440–451. https://doi.org/10.1111/gfl.12162 v.

Ziegler, P., 1990. Collision related intra-plate compression deformations in Western and Central Europe. J. Geodyn. 11 (4), 357–388. https://doi.org/10.1016/0264-3707(90)90017-o v.